Differences in evolutionary accessibility determine which equally effective regulatory motif evolves to generate pulses

Kun Xiong[*,†], Mark Gerstein[†,‡,§,**], Joanna Masel[††]

[*] Department of Molecular and Cellular Biology, University of Arizona, Tucson AZ, 85721

[†] Department of Molecular Biophysics and Biochemistry, Yale University, New Haven CT, 06511

[‡] Program in Computational Biology and Bioinformatics, Yale University, New Haven CT, 06511

[§] Department of Computer Science, Yale University, New Haven CT, 06511

[**] Department of Statistics and Data Science, Yale University, New Haven CT, 06511

[††] Department of Ecology and Evolutionary Biology, University of Arizona, Tucson AZ, 85721

Running title:

Non-adaptive evolution of network motifs

Keywords:

Pulse generation, adaptationism, mutation-biased adaptation, gene regulatory network, transcriptional regulation

Corresponding authors:

Mark Gerstein, Bass 432A, 266 Whitney Avenue, New Haven, CT 06511. Phone: 203-432-6105, E-mail: mark.gerstein@yale.edu

Joanna Masel, Department of Ecology and Evolutionary Biology, University of Arizona, 1041 E. Lowell St., Tucson, AZ 85721. Phone: 520-621-1588, E-mail: masel@arizona.edu

ABSTRACT

Transcriptional regulatory networks (TRNs) are enriched for certain "motifs". Motif usage is commonly interpreted in adaptationist terms, i.e. that the optimal motif evolves. But certain motifs can also evolve more easily than others. Here, we computationally evolved TRNs to produce a pulse of an effector protein. Two well-known motifs, type 1 incoherent feed-forward loops (I1FFLs) and negative feedback loops (NFBLs), evolved as the primary solutions. Which motif evolves more often depends on selection conditions, but under all conditions, either motif achieves similar performance. I1FFLs generally evolve more often than NFBLs, unless we select for a tall pulse. I1FFLs are more evolutionarily accessible early on, before the effector protein evolves high expression; when NFBLs subsequently evolve, they tend to do so from a conjugated I1FFL-NFBL genotype. In the empirical *S. cerevisiae* TRN, output genes of NFBLs had higher expression levels than those of I1FFLs. These results suggest that evolutionary accessibility, and not relative functionality, shapes which motifs evolve in TRNs, and does so as a function of the expression levels of particular genes.

INTRODUCTION

The topology of transcriptional regulatory networks (TRNs) is enriched for certain motifs (Lee et al. 2002; Milo et al. 2002; Shen-Orr et al. 2002; Mangan and Alon 2003). Many argue that these motifs are the result of adaptive evolution where the motif whose dynamical behavior best provides the beneficial function is the one that will evolve (Alon 2007). However, adaptationist claims about TRN organization have been accused of being just-so stories, with adaptive hypotheses still in need of testing against an appropriate null model of network evolution

(Wagner 2003; Artzy-Randrup et al. 2004; Mazurie et al. 2005; Kuo et al. 2006; Solé and Valverde 2006; Lynch 2007; Knabe et al. 2008; Jenkins and Stekel 2010; Tsuda and Kawata 2010; Widder et al. 2012; Ruths and Nakhleh 2013; Payne and Wagner 2015). We recently generated such a null model and used it to show that coherent type 1 feed-forward loops can, as hypothesized, evolve adaptively in response to selection to filter out short spurious signals, by combining a fast signaling pathway and a slow signaling pathway with an AND gate (Xiong et al. 2019). Testing the hypothesis in this way was not merely confirmatory, but generated other insights about the existence and nature of alternative adaptive solutions, especially when slow transcriptional regulation is combined with faster response mechanisms such as post-translational regulation (Xiong et al. 2019). Other network motifs and properties have not yet received similar treatment.

At least three different motifs (**Fig. 1A**) are all capable of producing a sharp pulse of expression in response to an increase in input signal (**Fig. 1B**) (Basu et al. 2004; Camas et al. 2006; Çağatay et al. 2009). All depend on an effector first being rapidly activated by a signal, and later, at a slower timescale, being repressed by it. These three motifs are simple auto-repression (AR), negative feed-back loops (NFBLs), and incoherent type 1 feed-forward loops (I1FFLs) (**Fig. 1A**). The three motifs are topologically and functionally similar to each other, differing in whether the slow repression is effected via negative autoregulation by the effector *R* of itself, via negative feedback regulation of *R* using a specialized repressor, or via a separate negative control pathway from the input to the repressor and then the effector.

71 The high prevalence of I1FFLs and NFBLs in TRNs has been interpreted to occur because these
72 two motifs are adaptations for pulse generation and closely related functions (Shoval and Alon
73 2010; Shoval et al. 2010; Ferrell 2016; Shi et al. 2017). Both I1FFLs and NFBLs allow the steady-
74 state level of the effector, before and after the pulse, to be independent of the signal strength,
75 a property known as chemical adaptation (Ferrell 2016; Shi et al. 2017). We note that AR is
76 normally hypothesized to perform functions other than pulse generation (Wall et al. 2004; Alon
77 2007), but theoretical analysis and experiments show that AR can generate pulses (Rosenfeld et
78 al. 2002; Camas et al. 2006; Amit et al. 2007). We therefore include AR for the completeness of
79 the study, while focusing on I1FFLs and NFBLs.
80
81 Which of the motifs is likely to evolve is often explained by adaptive demands for specific
82 properties of the pulse. For example, although both I1FFLs and NFBLs allow the amplitude of
83 the pulse to be a function of the fold-change of the signal's strength (Shoval et al. 2010), they
84 do so with different functional forms (Adler et al. 2014). I1FFLs and NFBLs can also differ in their
85 ability to filter noise in the signal (Buzi and Khammash 2016).
86
87 Alternatively, non-adaptive causes might be responsible for differences in the occurrence of the
88 three motifs. An important non-adaptive consideration is that fitness landscapes tend to have
89 many alternative local endpoints, which might take the form either of peaks (Whitlock et al.
90 1995) or of plateaus (van Nimwegen and Crutchfield 2000). Factors such as expression levels
91 can change the relative accessibility of different local evolutionary endpoints, in ways that are
92 independent of differences in their heights. Note that by "non-adaptive" explanations, we do

not mean "neutral evolution". Instead we refer to evolutionary accessibility, encompassing both which mutations occur in a single step and which hill-climbing multi-step paths are possible. This emphasis on *process* as non-adaptive explanation is in contrast to adaptive explanations that consider only the optimality of the final evolutionary *outcome*. Whether the non-adaptive explanation of evolutionary accessibility is a plausible cause is a question that *in silico* evolution is ideally set up to explore. We note that I1FFLs and NFBLs differ by whether it is the signal or the effector that regulates the repressor (**Fig. 1A**). Intuitively, the relative ease of evolving these two possible regulatory interactions with the repressor could depend on the relative expression levels of the candidate regulators.

Here we simulate TRN evolution under selection to produce a pulse, and test how subtle differences between scenarios might have both adaptive and non-adaptive effects on which motifs evolves. In particular, a highly expressed effector is more able to stimulate its repressor, and we therefore predict that this scenario should be more likely to evolve regulation via an NFBL and correspondingly less likely to evolve an I1FFL. Our simulations reject adaptationist explanations – I1FFLs and NFBLs achieve similar fitness – and confirm that NFBLs are evolutionarily more accessible than I1FFLs under this scenario, but that I1FFLs are more accessible under other scenarios where a highly expressed effector is not required. Data from real-world yeast TRNs agree with model predictions, showing that the effectors of NFBLs generally have higher expression levels than those of I1FFLs.

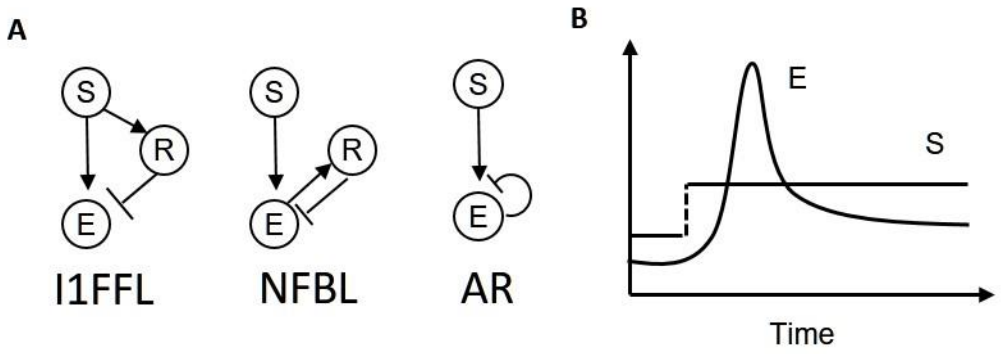

Figure 1. Three motifs (I1FFL, NFBL, and AR) all produce a pulse of effector E expression in response to increased signal S. (A) In all three cases, rapid and direct activation of the effector by the signal is eventually countered by a slower path of repression. The three motifs differ topologically in whether repression is by the effector itself (AR), by a specialized repressor (R) that is activated by the signal (I1FFL), or by a specialized repressor that is activated by the effector (NFBL). Regular arrow tips represent activation and ⊣ represents repression. **(B)** With appropriate parameters, and with a delay between transcriptional activation and protein production in the case of AR, all three motifs can induce a pulse, as the initial increase in expression as S activates E is eventually tamped down by a path of repression.

MATERIALS AND METHODS

Transcriptional regulation

Transcription factors (TFs) bind to a given TF binding site (TFBS) according to a formula based on the biophysics of the matching of the cis-regulatory sequence to the TF's consensus binding sequence (see Supplementary Materials/TF binding for details). Briefly, in isolation from all other TFs and TFBSs, the probability P_b that a TFBS is occupied is

$$P_{\mathrm{b}} = \frac{C}{\bar{K}_{\mathrm{d}} + C}$$

where C is the total concentration of the TF and $\widehat{K}_d$ is a version of the binding affinity K_d of the TF, rescaled to account for the fact that focal TFBSs must compete for TF with many non-specific binding sites throughout the genome. From probabilities of this form, we calculate the probability that exactly A activators and R repressors are bound to a given cis-regulatory sequence, given the possibility of physical overlap among TFBSs (see Supplementary Materials/TF occupancy). From this, we derive four probabilities that we assume regulate gene expression: 1) the probability P_A of having at least one activator bound to a gene, 2) the probability P_R of having at least one repressor bound, 3) the probability $P_{\text{A\_no\_R}}$ of having no repressors and one activators bound, and the probability $P_{\text{notA\_no\_R}}$ of having no TFs bound.

We model transcriptional initiation as a two-step process whose rates depend on TF binding, and parameterize those rates with reference to nucleosome disassembly followed by transcription machinery assembly (Mao et al. 2010; Brown et al. 2013). We model a repressed state of nucleosome presence, an intermediate state of a nucleosome-free transcription start site that lacks transcription machinery, and an active state. We set the transition rate from the repressed state to the active state to

$$r_{\text{Rep\_to\_Int}} = 0.92P_{\text{A}} + 0.15(1 - P_{\text{A}}),$$

using as bounds for our linear function 0.15 min^{-1} as the background rate of histone acetylation (Katan-Khaykovich and Struhl 2002) (which leads to nucleosome disassembly) and 0.92 min^{-1} as the rate of nucleosome disassembly for the constitutively active PHO5 promoter (Brown et al. 2013).

We set the transition rate from the intermediate state to the active state to

$$r_{\text{Int\_to\_Rep}} = 4.11P_{\text{R}} + 0.67(1 - P_{\text{R}}),$$

where 0.67 min^{-1} is a background histone de-acetylation rate (Katan-Khaykovich and Struhl 2002) and 4.11 min^{-1} is chosen so as to keep a similar maximum:basal rate ratio as that of $r_{\text{Rep\_to\_Int}}$.

We assume that the binding of a single repressor can prevent the transition from the intermediate state to the active state (Courey and Jia 2001). In the absence of repressors, activators facilitate the assembly of transcription machinery (Poss et al. 2013). Under these assumptions, we set the transition rate from the intermediate state to the active state to

$$r_{\text{Int\_to\_Act}} = 3.3P_{\text{A\_no\_R}} + 0.025P_{\text{notA\_no\_R}},$$

where 3.3 min^{-1} is the rate of transcription machinery assembly for a constitutively active *PHO5* promoter (Brown et al. 2013), and 0.025 min^{-1} is same rate when the *PHO4* activator of the *PHO5* promoter is knocked out.

We set the transition rate $r_{\text{Act\_to\_Int}}$ from the active state to the intermediate state to be gene-specific and independent of TF binding. This is because the promoter sequence not only determines which specific TFBSs are present, but also influences non-specific components of the transcriptional machinery (Decker and Hinton 2013). See Supplementary materials/$r_{\text{Act\_to\_Int}}$ for the parameterization of $r_{\text{Act\_to\_Int}}$.

Fitness

Our simulations of gene expression begin with a burn-in phase of random length, to ensure that TRNs to respond to a change in the signal, rather than evolve a timer mechanism. The level of

signal is low during the stage one burn-in, which lasts for 120 + x minutes, where x is random number drawn from an exponential distribution truncated at 30, and with an un-truncated average of 10. Fitness is assessed only on the basis of stage two, which lasts for 240 minutes, plus the last 5 minutes of stage one. We sample the effector concentration at one-minute intervals. The highest effector concentration during stage two is denoted p.

The fitness of a TRN has four components: the peak level of effector, a low effector expression starting point, the speed with which effector expression rises, and the speed with which it falls. Together, these four components capture the core attributes of what it means to be a pulse, and in combination, they apply consistent selective pressure first to generate any pulse at all and later to produce a superior pulse. All four fitness components are based on the expression level of the effector. For the purpose of scoring effector concentration and hence fitness, we use the total protein level of all effector proteins, including those that have diverged, following duplication, to have different regulatory activities.

Fitness component one scores the match to a pre-defined peak effector expression level:

$$f_1 = e^{-\frac{(log(p)-log(p_{opt}))^2}{\sigma^2}}. \quad (1)$$

We set the optimal peak expression level p_{opt} to 5,000 molecules per cell, 10,000 molecules per cell, or 20,000 molecules per cell, corresponding to selection for a low, medium, or high peak level, respectively. Under the assumption that the effector is a metabolism-related protein, we

chose the number 10,000 based on the average number of PDC1 protein molecules per yeast cell (Ghaemmaghami et al. 2003). The effector also acts as TF; this kind of dual functionality is not uncommon in yeast (Gancedo and Flores 2008). We set $\sigma^2 = 0.693$ so that when p = $0.5p_{opt}$, $f_1 = 0.5$.

We set fitness component two to reward low effector expression at the end of stage one:

$$f_2 = \begin{cases} \frac{p - s_1}{0.9p}, s_1 > 0.1p \\ 1, s_1 \leq 0.1p \end{cases}, \quad (2)$$

where s_1 is the arithmetic mean of the effector level across the last 5 minutes of stage one. This is chosen as a simple piecewise-linear function, which plateaus at a maximum of 1 for values of s_1 below 10% of the peak level p.

We set fitness component three to reward rapid turn-on of effector:

$$f_3 = \begin{cases} \frac{240 - t_{half\_peak}}{240 - t_{saturate}}, t_{half\_peak} > t_{saturate} \\ 1, t_{half\_peak} \leq t_{saturate} \end{cases} \quad (3)$$

where t_{half_peak} is the latest time in stage 2 at which the effector level is at $0.5(s_1 + p)$ before the effector hits its peak, and $t_{saturate}$ sets a time for which making effector response still more rapid no longer increases fitness. We set $t_{saturate}$ to 60 minutes.

To select for the downward slope of a pulse, fitness component four rewards falls in the effector falls to no more than 80% of the peak level by the end of stage two:

$$f_4 = \begin{cases} \frac{p - s_4}{0.2p}, s_4 \geq 0.8p \\ 1, s_4 < 0.8p \end{cases} \quad (4)$$

where s_4 is the arithmetic mean of the effector level across the last 5 minutes of stage two. Again, we chose a piecewise-linear function. We chose the relatively high value of 80% in order to select for an inclusive category of pulses. We consider pulses that eventually return all the way down to the level that prevailed before the signal (i.e. biochemical adaptation) to be a special case.

In some simulations of gene expression, we observed a peak expression level that is smaller than or equal to the effector's expression level right before the signal increases, or is even 0. In neither of these cases do fitness components Eq. 2 and/or 4 provide a useful selection gradient toward the evolution of a pulse. For simplicity, we set the fitness of these two cases to zero.

In addition to the selection described above to favor a pulse, at each point in the simulation, gene expression also incurs a cost that is proportional to the total rate of translation of all genes (see Supplementary Materials/Cost of gene expression). The estimated fitness of a TRN from one gene expression simulation is the arithmetic mean of the four components minus the cumulative cost of gene expression throughout the last 360 minutes of a simulation of gene expression.

Evolution

We calculate the arithmetic mean fitness $f_{resident}$ of the current ("resident") TRN across 1000 replicate simulations of gene expression, and the arithmetic mean fitness f_{mutant} of the mutant across 200 replicate simulations of gene expression. If f_{mutant} satisfies

$$\frac{f_{mutant} - f_{resident}}{|f_{resident}|} \geq 10^{-8}, \quad (5)$$

we replace the resident TRN with the mutant, and re-calculate the fitness of the new resident TRN to higher resolution using an additional 800 replicate simulations of gene expression.

Because gene expression is stochastic in our simulations, estimated fitness varies among replicates, and is subject to error even after averaging across many replicates. This means that our algorithm allows neutral or slightly deleterious mutations to fix. This is sometimes even explicit; the updated fitness that includes 800 additional simulations of the successful mutant can be lower than the fitness of the TRN it replaced.

Standard origin-fixation evolutionary simulations explicitly calculate a probability of fixation for each mutation and compare it to a pseudo-random number to decide whether fixation occurs. Our model achieves a similar exploration of nearly neutral evolutionary paths by using the intrinsic uncertainty in the stochastic estimation of fitness. Our approach wastes as few beneficial mutations as possible, minimizing computation, rather than discard most beneficial mutations through the use of a fixation probability that is only around twice the selection coefficient (Haldane 1927). For example, in our simulations, we accepted 0.5 million out of 1.9 million trialed mutations across 10 evolution replicates in the high-peak condition, of which

only a minority can be presumed to have achieved true fitness increases (**Fig. S1**). Importantly, fixation probability in our algorithm still depends on the size of the true underlying fitness difference, which controls the probability that the estimated selection coefficient in Eq. 5 will be positive.

Counting network motifs

We count I1FFLs and NFBLs formed by the signal, an effector gene, and a repressor gene that is different from the effector gene, with interactions between them as shown in **Fig. 1A**. We count ARs formed by the signal and an effector gene. We score gene A as potentially regulating gene B, i.e. creating one of the links shown in **Fig. 1A**, if there is a TFBS for A in the cis-regulatory sequence of B. We allow genes in I1FFLs and NFBLs to self-regulate. An overlapping I1FFL in which the effector and the auxiliary TF repress each other is counted not as two I1FFLs, but rather as a different (and rarer) type of network motif. Overlapping I1FFLs evolve rarely.

Given that two mismatches to an 8-bp consensus sequence still yield above-background binding, a random 8-bp sequence qualifies as a weak affinity TFBS with probability $\binom{8}{2} \times 0.75^2 \times 0.25^6 = 0.0038$. Each cis-regulatory sequence contains around 300 8-bp potential binding sites (including both orientations of a 150 bp cis-regulatory sequence), among which 1.14 will on average qualify by chance as a two-mismatch TFBS for a given TF. These two-mismatch TFBSs, occurring so often by chance, usually have low affinity, and therefore might have little regulatory effect. It is for this reason we refer to them above as potential regulatory interactions – our previous work has shown that motifs can appear more clearly when weak

affinity TFBSs with little regulatory effect are excluded (Xiong et al. 2019). Four types of spurious two-mismatch TFBSs can create apparent but non-functional I1FFLs and NFBLs: S → TF, E → TF, TF → E, and E → E (**Fig. S2**), where "TF" refers here to a transcription factor that is not an effector. Because it is computationally expensive to test whether each two-mismatch TFBS is spurious, we instead tested all cases at a time for each of the four types listed above. Specifically, we recalculate the fitness of the TRN while ignoring all 2-mismatch TFBSs of that type, across 1,000 gene expression simulations, and deem the entire set of TFBSs spurious if the recalculated fitness is at least 99% of the original fitness (see **Fig. 2** legend for variations on this criterion). We ignore spurious connections while scoring network motifs.

Mutations that create and destroy motifs

For each evolutionary replicate, we identified the evolutionary steps at which the number of instances of a given motif changes to or from zero, which we call "motif-destroying-mutations" and "motif-creating-mutations", respectively. We removed spurious TFBSs before scoring motifs, as described in the last section, with one modification: to save computation related to mutations that were trialed and then rejected by selection, we used only 200 gene expression simulations to determine fitness without the TFBS in question, with a threshold of 98% of original fitness. Mutations that change the expression levels of a gene and/or the binding affinity of a TF can potentially change whether a two-mismatch TFBS is "spurious" in terms of fitness effects, effectively rewiring the TRNs even if they do not create or destroy core TFBSs of the motif in question.

Expression levels of TFs in yeast TRN

We used YeastMine (Balakrishnan et al. 2012) to retrieve 129 *S. cerevisiae* genes that have the GO term "DNA-binding transcription factor activity" or children of this GO term. We then searched Yeastract (Teixeira et al. 2006) for TFs that regulate these 129 TFs, demanding evidence from both DNA binding and gene expression. When the search found new TFs that are not included in list given by YeastMine, the new TFs were added to the list and fed to Yeastract again. We stopped the iterative search when no new TFs were found, and the final list has 203 TFs. Yeastract annotates interactions between pairs of TFs as activating, repressing, or both. When annotated as "both" (i.e. likely condition-specific), we interpreted it as whichever interaction mode would be needed in order to complete a motif. We scored I1FFLs, NFBLs, and their conjugates from all combinations of three TFs out of the 203, allowing E and/or R to be self-repressing. Because the effectors of NFBLs must be activators, we excluded I1FFLs whose effectors are repressors in case there is a systematic difference in expression between activators and repressors. In total, we identified 46 NFBLs, 30 I1FFLs, and 7 I1FFL-NFBL conjugates.

To assess peak expression level, we used the data of Gasch et al. (2000), who applied multiple stimuli to yeast and measured the fold-change in RNA expression of all genes relative to pre-stimulus expression levels. We analyzed data on exposure to 10 stimuli: amino acid starvation, nitrogen depletion, sorbitol osmotic shock, temperature shift from 25° to 37°, diamide, hydrogen peroxide, menadione disulfate, diauxic shift, dithiothreitol, and transition to a stationary phase of growth. Following each stimulus, fold-change was recorded over several

time points. We consider an effector gene to exhibit pulse-like expression if the maximum fold-increase in expression occurs prior to the last time point and has a larger magnitude than that of the maximum fold-decrease in expression; we excluded gene-stimulus combinations that do not meet this criterion from further analysis. For input and repressor genes, we did not require a pulse, but merely that the stimulus led to increased expression (measured as average fold-change across time points), and that the maximum fold-increase was larger than the maximum fold-decrease. We excluded repressor-stimulus and input-stimulus combinations that failed to meet both criteria.

We note that the same gene can occupy the same position within multiple motifs. For example, GAT1 is the effector in 18 NFBLs and one I1FFL, suggesting that this gene might be particularly well-suited for function within NFBLs. To compare gene expression between I1FFLs and NFBLs, we weighted the fold-change in expression of a given gene by the frequency with which that gene appears in the motif of interest, e.g. weights of 18/19 and 1/19 for GAT1's appearance as an effector in NFBLs and I1FFLs, respectively. For I1FFL-NFBL conjugates, we assign half-weights to both I1FFLs and NFBLs.

We complemented this peak-RNA-expression analysis with an analysis of the average protein levels (i.e. not peak levels), taken from PaxDB (Wang and Purisima 2005). One analysis is restricted to a March 2013 data set originally compiled by PeptideAtlas (Desiere et al. 2006) to show the abundances of peptides in *S. cerevisiae* pooled across 90 experiments, which include normal growth conditions and perturbed growth conditions, e.g. cell cycle arrest and metabolic

355 perturbation. We also used another data set "GPM, Aug, 2014" from PaxDB, which has more
356 genes than "PeptideAtlas, March 2013" (5289 versus 4828). While we could not find a detailed
357 description for this GPM (the Global Proteome Machine) (Craig et al. 2004) dataset, GPM
358 generally includes data from PeptideAtlas (Craig et al. 2004), meaning that this data similarly
359 includes both normal growth conditions and perturbed growth conditions. Weighted average
360 protein levels were calculated with the same weighting scheme as for fold-change of gene
361 expression.
362
363 **Data Availability**
364 The source code for our computational model is available at
365 https://github.com/MaselLab/network-evolution-simulator/tree/I1_FFLs.
366
367 **RESULTS**
368 **Model overview**
369 We used a previously described computational model to simulate the expression of genes in a
370 TRN, parameterized by available *Saccharomyces cerevisiae* data (Xiong et al. 2019). **Fig. S3**
371 summarizes the model, and the model parameters are summarized in **Tables S1** and **S2**. The
372 TRN evolves under a realistic mutational spectrum including *de novo* appearance of weak-
373 affinity TFBSs, and frequent gene duplication and deletion. Briefly, each gene in the TRN
374 encodes either an activating or repressing TF, and each is regulated by a 150-bp cis-regulatory
375 sequence accessible to TF binding. Each TF recognizes an 8-bp consensus binding sequence with
376 a characteristic binding affinity. Binding sites with up to two mismatches are still recognized,

with each mismatch reducing binding affinity according to a thermodynamic model (Supplementary Materials/TF Binding). TFs can bind in either orientation. Each TF that binds to DNA occupies three extra base pairs upstream and downstream of the consensus sequence, making a total of 14 bp inaccessible to other TFs. The concentrations of TFs are used to calculate the probabilities that each cis-regulatory region is bound by a given number of activators and repressors (see Methods).

To simulate gene expression, we assume that each gene transitions between an active chromatin state that can initiate transcription, an intermediate primed state capable of becoming either activated or repressed, and a repressed chromatin state. Most transition rates depend on whether activators and/or repressors are bound (see Methods), with the fastest transition rate to the active state occurring when at least one activator and no repressors are bound. The transcription initiation rates of mRNAs from active genes are gene-specific, and so are the degradation rates. Note that the above rates (including the transition rates between the states of genes) are expectations; exactly when a reaction (e.g. one of gene A's mRNAs is degraded) happens is simulated stochastically using a Gillespie algorithm (Gillespie 1977). Conceptually, the algorithm allows one event to happen at a time, with the cellular state remaining unchanged between events. The waiting time between two events has an exponential distribution, with a mean specified by the total reaction rates. Once the time of an event is sampled, the algorithm randomly picks an event (e.g. degrading gene A's mRNA) based on the reaction's relative rate, and changes the cellular state according to the event (e.g. there is one less mRNA of gene A in cell). See Supplementary materials for details.

Each mRNA produces protein at a gene-specific translation rate. Once transcription is initiated, we simulate a delay before mRNA can be translated at full speed. The delay accounts for the completion of both transcription and the loading of ribosomes to mRNA, and is a function of gene length (Supplementary materials/Transcriptional delay and Translational delay). Because tracking the turnover of individual protein molecules with a Gillespie algorithm is computationally expensive, we calculate the turnover of proteins with ordinary differential equations (Supplementary materials/Simulation of gene expression).

To select for pulse generation, we designate an input signal to the TRN, which binds to cis-regulatory regions like any other TF, but whose concentration is set externally rather than being regulated by other TFs in the TRN. The input signal always activates gene expression. Signal concentration is low and constant during a burn-in phase, where genes are initialized with a repressed chromatin state, and begin with zero non-signal mRNA and protein. Then in stage 2, the signal instantly switches to a high level, and selection is applied for a TF designated to be the “effector” to exhibit pulse-like expression. High fitness depends on having low effector expression at the end of stage 1, matching a pre-defined peak effector concentration during stage 2, rapidly increasing effector level after stage 2 begins, and having a low effector level at end of stage 2. Details of the signal and fitness calculation are given in the Methods.

We initialize an evolutionary simulation with a randomly generated genotype of 3 activator genes, 3 repressor genes, and an effector gene. The effector is initialized as an activator, which

makes NFBLs more accessible than ARs (although below we will explore the effects of switching this). All quantitative gene-specific parameter values, such as transcriptional rates and gene length, are randomly initialized according to empirically estimated distributions (see **Table S1** and Supplementary materials).

We simulate five classes of mutations. **Table S2** lists the corresponding mutation rates and details of the parameterization are provided in the Supplementary materials. A class-one mutation is a duplication or deletion of one gene along with its cis-regulatory sequence. The maximum number of genes is capped at four effector genes plus 21 non-effector genes (excluding the signal) to limit computational cost. Once this limit is reached, no duplication mutations are allowed. In addition, once any give gene is present in four copies, none of the copies are duplicated until one is again lost by deletion. Neither the last effector gene nor the last non-effector gene are subject to deletion. The signal is subject neither to duplication nor to deletion.

Class-two mutations are single nucleotide substitutions in the cis-regulatory sequences, which can cause TFBS turnover. Mutations change one nucleotide to one of the other three nucleotides with equal probabilities.

Class-three mutations change quantitative gene-specific parameters, i.e. the rate at which transcriptional bursts end, gene length, mRNA degradation rate, protein synthesis rate, protein degradation rate, and the affinity of a TF to DNA. All quantitative gene-specific parameters

except length are subjected to mutational bias, e.g. mutation tends to reduce the affinity of TF binding. In case this is insufficient to ensure the values of the mutatable parameters never go beyond reasonable limits, we also apply hard bounds (see Supplementary materials/Mutations for details).

Class-four mutations convert transcription activators to repressors (or the reverse). This mutation does not apply to the input signal, i.e. the input signal is always an activator.

Class-five mutations change a single nucleotide preference in a TF's consensus binding sequence. One of the other three nucleotides is chosen for the consensus binding sequence with equal probabilities.

When gene duplicates differ due only to class-three mutations, the duplicates are considered as "copies" of the same gene, encoding "protein variants". Once a class-four or class-five mutation is applied to a gene duplicate, the duplicate becomes a new gene encoding a new protein. When scoring motifs, we require that each node be a different protein.

Evolution is simulated using the revised origin-fixation model introduced by Xiong et al. (2019). Briefly, the resident genotype experiences one mutation, chosen according to the relative rates of all possible mutations. The fitness of the original resident TRN and of the mutant TRN is calculated by simulating gene expression in response to an input signal (see Methods for details). If the estimated fitness of the mutant is sufficiently high (see Methods for details), the

mutant replaces the resident genotype. Note that estimated fitnesses include stochasticity from the simulation of gene expression, which serves to introduce a form of genetic drift. If no replacement occurs, we generate a new mutant and repeat the procedure until a replacement is found. We call a replacement an evolutionary step, and end each simulation after 50,000 evolutionary steps. We use the average fitness of the last 10,000 evolutionary steps to determine whether evolution has found a good solution.

High peak expression level non-adaptively promotes NFBLs

We evolve TRNs under selection to generate a pulse of effector expression in response to a sudden 10-fold increase in input. While any of the three network motifs can solve this challenge, a highly expressed effector is more capable of stimulating its repressor, and thus this solution should be more likely to evolve regulation via an NFBL and correspondingly less likely to evolve an I1FFL. Note that this prediction is expected on both adaptive grounds of which solution might be superior, and on non-adaptive grounds of which solution is easier for evolution to find.

To test this prediction, we vary the optimal peak level of the effector (see Methods for details of fitness function). *In silico* evolution from a random starting point is not always successful at reaching the target phenotype, so we focus on the most evolutionarily successful simulations. We do this by dividing evolutionary replicates into three categories based on final fitness (**Fig. S4**). See **Fig. S5** for examples of the phenotypes of the high-fitness replicates.

High-fitness solutions rarely involve AR under any of the three selection conditions, while both I1FFLs and NFBLs evolve often (**Fig. 2A**). As predicted, when we select for higher effector expression, we get more NFBLs and fewer I1FFLs (**Fig. 2A**). These NFBLs were absent from medium-fitness solutions, which instead employed I1FFLs or ARs (**Fig. S9A**), generally achieving lower peak effector expression than in the high-fitness solutions (**Fig. S9B**). While this seems to suggest that NFBLs might be adaptively superior, if we prevent one type of motif from evolving, similarly high fitness genotypes can be obtained via the other motif (**Figs. 2B and S8**). The reason we get more NFBLs and fewer I1FFLs with selection for higher peak effector expression is therefore not straightforward adaptive superiority of the former, but rather the relative ease of finding high-fitness solutions.

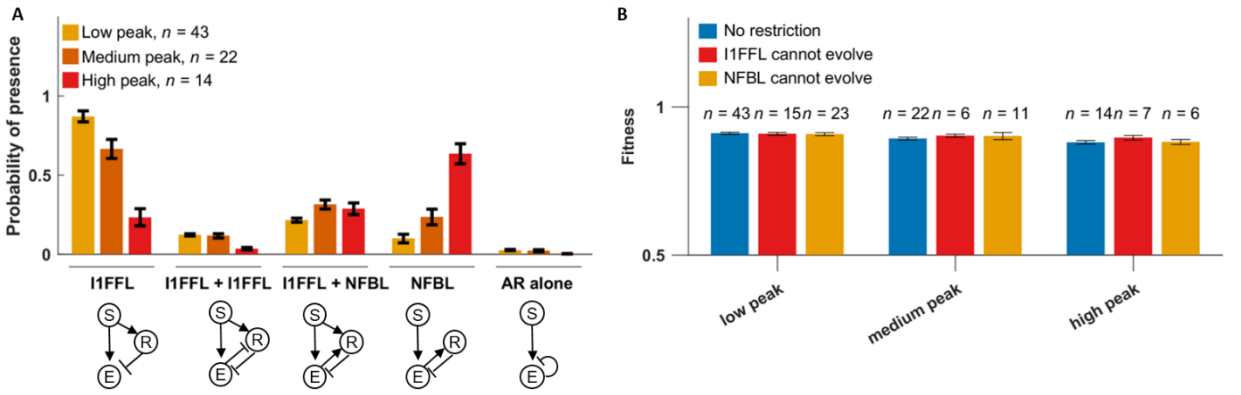

Figure 2. Selection for high peak effector expression levels promotes NFBLs. (A) TRNs are evolved under selection to generate pulses in response to an input signal. Under all three selection conditions, the input signal starts with 100 molecules per cell and increases to 1,000 molecules per cell to trigger a pulse. Three versions of the evolutionary simulations select for three different optimal peak effector levels of the effector: low (P_{opt} = 5,000 molecules per cell),

504 medium (P_{opt} = 10,000 molecules per cell), and high (P_{opt} = 20,000 molecules per cell). For each
505 high-fitness genotype (**Fig. S4**), we calculate the proportion of evolutionary steps that contain
506 at least one network motif of the specified type among the last 10,000 evolutionary steps (out
507 of a total of 50,000 evolutionary steps). When scoring for motifs, non-functional spurious TFBSs
508 were excluded (see Methods for details, and **Fig. S6** for results using different TFBSs exclusion
509 criteria). R can be auto-regulating (not shown in circuit diagram). On rare occasions, AR co-
510 occurred with I1FFLs or overlapping I1FFLs (labelled here I1FFL + I1FFL) (**Fig. S7**), and these few
511 cases were included in the scoring of I1FFL and overlapping I1FFL frequencies. **(B)** Preventing
512 either NFBLs or I1FFLs from evolving does not lower the final fitness within high-fitness
513 evolutionary simulations. Instead, genotypes obtained equally high fitness by evolving the other
514 common motif (**Fig. S8**). To prevent NFBLs from evolving, we remove the TF binding activity of
515 effectors; this also prevents the evolution of the AR auto-repression motif. To prevent I1FFLs
516 from evolving, we ignore TFBSs for the signal in the cis-regulatory sequence of any repressors.
517 Because this might have unintended consequences for mutations that convert repressors
518 to/from activators, we set to zero the rate of mutations that effect this conversion. Data are
519 shown as mean ± SE over replicates.
520
521 **Early bias toward I1FFLs can shift to later NFBL evolution via I1FFL-NFBL conjugates**
522 The combined frequency of the two motifs rises throughout the long period of evolution, rather
523 than topological solutions being found early and becoming locked in and only incrementally
524 improved on. However, the frequency of I1FFLs in particular rises prominently during the first

10,000 evolutionary steps (**Fig. 3**), even under selection for high peak effector levels, i.e. selection that ultimately leads to an evolutionary preference for NFBLs (**Fig. 3C**).

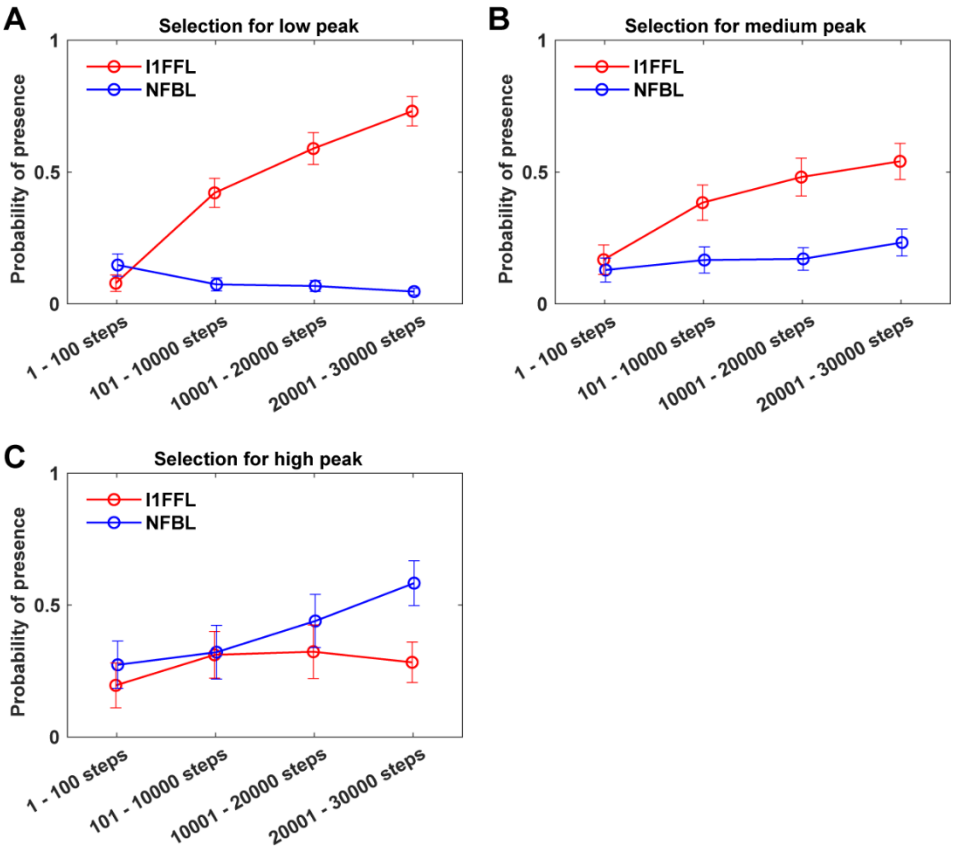

Figure 3. Evolution of I1FFLs and NFBLs follow different trajectories. We score motif occurrence during different time periods along the way to the evolution of the high-fitness replicates shown in **Fig. 2A**. See **Fig. S10** for the occurrence of other motifs during evolution. As in **Fig. 2A**, we calculated the proportion of evolutionary steps that contain at least one network motif of the specified type. Note that because some evolutionary replicates oscillate between motif presence and absence, given the potential for slightly deleterious mutations in our evolutionary algorithm, the fraction of evolutionary replicates that frequently show the

536 motif in question is higher than the probability of presence in one evolutionary step as shown
537 here. Data are shown as mean ± SE over replicates.
538
539 To further test this point, we made the early evolution of NFBLs less accessible by initializing
540 the effector as a repressor. While this reduced the frequency of NFBLs even under selection for
541 a high peak, those NFBLs that still evolved reached similar performance to I1FFLs (**Fig. S11**). This
542 further supports early evolutionary accessibility as a key factor.
543
544 The relative ease of I1FFL evolution could be because more mutations create I1FFLs and/or
545 because mutations creating I1FFLs have higher acceptance rates. To explore this further, we
546 characterize the mutations that create I1FFLs and/or NFBLs in TRNs that do not currently
547 contain such a motif. I1FFL-creating mutations occur at a higher rate than NFBL-creating
548 mutations under selection for low-peak and medium-peak expression, while NFBL-creating
549 mutations are more common under selection for high-peak expression **(Table 1)**. The rarity of
550 NFBL-creating mutations becomes much more pronounced when we restrict our analysis to
551 mutations that do not also destroy or create another motif – this tendency holds even under
552 conditions that favor NFBLs, i.e. late in evolution under selection for high-peak expression
553 (**Table 1**). Greater mutational accessibility of the I1FFL motif is clearly one of the factors
554 favoring this motif.
555
556 The early evolution of I1FFLs is also facilitated by the higher acceptance rate of I1FFL-creating
557 mutations relative to NFBL-creating mutations, particularly during the first 10,000 evolutionary

steps (**Table 1)**. Similarly, I1FFL-destroying mutations are accepted less often than NFBL-destroying mutations are, in this case throughout the course of evolution and regardless of target peak expression (**Table S4**). Note that mutations that create one motif frequently destroy another, with NFBL-creating mutations more prone to this problem than I1FFL-creating mutations (**Table 2**). While some such disruptive mutations are accepted by our evolutionary algorithm (**Table 2**), acceptance rates are higher for non-disruptive mutations (**Table 1**). If we restrict our analysis to non-disruptive mutations, we see stronger mutation bias toward I1FFLs, and more similar acceptance rates for I1FFLs vs NFBLs (**Table 1**). In other words, a shortage of non-disruptive NFBL-creating mutations is an obstacle to the evolution of NFBLs. NFBL-creating mutations that destroy I1FFL-NFBL conjugates are both more common and more likely to be accepted than NFBL-creating mutations that destroy I1FFLs (**Table 2**). This suggests that I1FFL-NFBL conjugates might be an important intermediate step in the evolution of NFBLs, rather than NFBLs evolving de novo. This makes sense; after early evolution of an I1FFL provides a partial solution to the selective challenge, the evolutionary path to an NFBL does not abandon that I1FFL solution, but instead passes through a combined I1FFL-NFBL intermediate. The evolutionary path from an early partial I1FFL solution might lead either to a superior I1FFL or to an NFBL, with the potential to achieve similarly high fitness in either case.

peak level		**Evolutionary step 1 – 10,000**				**Evolutionary step 10,001 – 30,000**			
		all mutations		non-disruptive mutations		all mutations		non-disruptive mutations	
		Trialed	Acceptance rate	Trialed	Acceptance rate	Trialed	Acceptance rate	Trialed	Acceptance rate
Low	I1FFL-creating	0.049	0.171	0.0038	0.606	0.077	0.142	0.0019	0.550

	NFBL-creating	0.026	0.078	0.00074	0.544	0.024	0.062	0.00028	0.504
Medium	I1FFL-creating	0.072	0.102	0.0031	0.607	0.088	0.083	0.00091	0.432
	NFBL-creating	0.043	0.097	0.00084	0.694	0.049	0.078	0.00032	0.507
High	I1FFL-creating	0.036	0.114	0.0017	0.546	0.039	0.063	0.00027	0.411
	NFBL-creating	0.097	0.072	0.0017	0.642	0.147	0.069	0.00026	0.476

Table 1. Summary of mutations that create I1FFLs and/or NFBLs. We identify the accepted and rejected mutations that increase the number of I1FFLs and/or NFBLs in a TRN to above zero (see Methods for details). Among these mutations, "non-disruptive mutations" are those that create the given motif but do not otherwise alter the numbers of I1FFL (when NFBLs are created), NFBLs (when I1FFLs are created), I1FFL-NFBL conjugates, overlapping I1FFLs, and auto-repressors. For each selection condition and evolutionary stage, we pooled the qualified mutations from all high-fitness replicates shown in **Fig. 2A**. The total numbers of mutations of the given type were normalized by dividing by the total number of mutations trialed in resident TRNs that did not already have the motif in question. The acceptance rate shown in the table is the number of accepted mutations across all replicates divided by the number of trialed mutations across all replicates. Pseudoreplication may be a concern here; if the initial TRN tends to create one motif over the other, this might be propagated at all subsequent time points for that evolutionary replicate. However, **Table S3** shows that the initial mutational bias of a TRN can flip at a later stage of evolution.

peak level		**Evolutionary step 1-10,000**				**Evolutionary step 10,001-30,000**			
		Destroys I-N conjugates	accept. rate	Destroys I or N	accept. rate	Destroys I-N conjugates	accept. rate	Destroys I or N	accept. rate
Low	I1FFL-creating	0.461	0.108	0.101	0.169	0.529	0.092	0.106	0.183
	NFBL-creating	0.924	0.060	0.443	0.037	0.883	0.048	0.443	0.034
Medium	I1FFL-creating	0.643	0.048	0.100	0.137	0.647	0.056	0.132	0.108
	NFBL-creating	0.920	0.082	0.314	0.051	0.928	0.070	0.280	0.053

High	I1FFL-creating	0.466	0.047	0.255	0.148	0.611	0.021	0.274	0.090
	NFBL-creating	0.962	0.060	0.307	0.051	0.962	0.064	0.234	0.047

Table 2. Most NFBL-creating mutations also destroy other motifs. A high fraction of trialed mutations that create a given motif also destroy I1FFL-NFBL conjugates, and many also destroy NFBLs (in the case of I1FFL-creating mutations) or I1FFLs (in the case of NFBL-creating mutations). Destructive mutations are accepted at significant rates. Qualified mutations are pooled across all evolutionary replicates. See Methods for details about the identification of mutations that create and/or destroy motifs.

Indeed, I1FFL-NFBL conjugates (and NFBLs) are also often converted by mutation into simple I1FFLs. However, under selection for high peak effector expression, the acceptance rate of such mutations decreases over evolutionary time (**Table 2**). Peak effector expression increases during evolution (**Fig. S12**); this could drive increased preference for the now more highly expressed effector rather than the signal to control the repressor. In medium-fitness evolutionary replicates, high peak effector expression is not achieved, and NFBLs rarely evolve (**Fig. S9**). By the same logic, we hypothesize that strengthening the input signal should promote I1FFLs even under selection for a high effector peak. This is indeed the case, with promotion in particular of the evolution of the I1FFL-NFBL conjugate (**Fig. S13**).

Highly expressed effectors tend to be regulated by NFBLs in yeast

Next we tested our model predictions about when I1FFLs vs. NFBLs tend to evolve. We identified NFBLs, I1FFLs and I1FFL-NFBL conjugates in the TRN of *S. cerevisiae*, using Yeastract annotations of regulatory interactions between TFs (see Methods). Using data from Gasch et al.

(2000), we identified genes that display pulse-like expression in response to an environmental stimulus, and the peak heights of the pulses (measured as the fold-change of RNA expression levels relative to the expression level before the stimulus). In agreement with our model prediction, the effectors of NFBLs reach higher peaks than those of I1FFLs following stimulus (**Fig. 4A**). However, the input signals of NFBLs increase their expression more in response to stimuli than do those of I1FFLs (**Fig. 4A**), which disagrees with our model prediction. We note that the 46 NFBLs in our dataset involve 26 unique genes as the input signal and 8 as the effector, while the 30 I1FFLs involve 14 signals and 9 effectors. This raises the possibility that the more diverse signal inputs of the NFBLs might contain more false positive hits.

We also analyzed yeast protein expression levels from PaxDB, averaged across multiple environmental conditions rather than measured in response to stimuli (see Methods). We found that effector TFs generally have higher expression in NFBLs than in I1FFLs (**Fig. 4B**). Note that the direction of causation is not known from the empirical data alone: when an effector already has high expression this might prompt the evolution of NFBL, or the presence of an NFBL might facilitate the evolution of high effector expression. The theoretical work presented here presents non-exclusive proof of principle in support of the former interpretation.

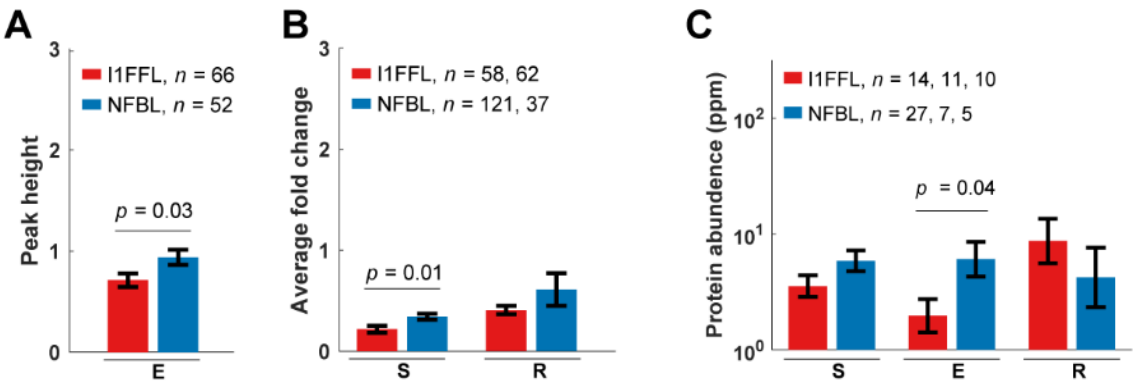

Figure 4. Effector TFs in yeast NFBLs have higher expression than those in I1FFLs. (A) Peak height of pulses was measured as the maximum fold-increase in RNA expression in response to one of 10 stimuli (see methods for details), for the subset of genes showing pulse-like RNA expression during the former in the RNA expression data of Gasch et al. (2000). **(B)** Average fold-change in signal and repressor RNA expression in response to stimuli, for the subset that showed an increase (see Methods). **(C)** Protein levels under normal conditions were taken from the "PeptideAtlas, March, 2013" dataset provided by PaxDB (Wang et al. 2015). A weaker result was obtained using a different dataset from PaxDB that includes a larger set of gene-environment combinations (**Fig. S14**). For fold-change in expression, data are shown as mean ± SE over each network position across all instances of the motif. The procedure is similar for protein abundance, except the data is first log transformed. For each motif, we list the numbers *n* of unique gene-stimulus combinations where pulse-like expression is observed at a signal node (S), effector node E, or repressor node R. p-values come from two-tailed t-tests.

DISCUSSION

We selected for a pulse generator in an evolutionary simulation model and observed which TRN motifs emerged. As predicted, selecting for high peak expression level of the effector promotes

NFBLs over I1FFLs, while a strong input signal promotes I1FFLs. However, if one motif is prevented from evolving, the other motif can evolve to take its place, with no loss of peak fitness, suggesting that the preference between motifs is not adaptive in origin, i.e. is not about which motif is optimal. One predicted pattern is confirmed in the actual TRN of *S. cerevisiae*, where the effector's expression level is higher in NFBLs than in I1FFLs.

Both mutational accessibility (i.e. how often mutations create the given motif) and selective acceptance rates (Yampolsky and Stoltzfus 2001; Stoltzfus and McCandlish 2017; Gomez et al. 2020) contribute to patterns of relative evolutionary accessibility. Note that the motif created by larger-effect beneficial mutations need not be better at generating a pulse. The latter is what is meant by an "adaptive" explanation for the dominance of I1FFL over NFBL (or the vice versa) (Gould and Lewontin 1979). A non-adaptive evolutionary explanation can include a role of selection or an increase in fitness during evolution, but emphasizes process rather than final fitness as the cause of bias in evolutionary outcomes.

Usually mutational accessibility and selective acceptance rates point in the same direction, but not always: I1FFLs are less mutationally accessible under early selection for high peak effector expression, but have a relatively high mutation acceptance rate. The higher acceptance rates for I1FFL-creating mutations do not reflect functional superiority of I1FFLs, but rather the fact that creating NFBLs frequently involves destroying other, likely functional, motifs. Avoidance of damage to existing functions has been previously noted in other discussions of the evolutionary paths taken by TRNs (Wagner 2003; Carroll 2008; Stern and Orgogozo 2009; Sorrells and

Johnson 2015). The mutational accessibility of different motifs is not static, but changes over the course of an evolutionary path (**Table S3**).

We did not pit the performance of I1FFLs and NFBLs versus the evolutionary accessibility of the two motifs, because both motifs had indistinguishable performance in our system. We are therefore unable to answer whether the evolutionary accessibility of motifs can alter the evolutionary outcome predicted by performance of motifs. However, finding in our system that high fitness solutions can often be found one way or another is intriguing in its possible generality.

We find that most NFBLs evolve not from connecting previously disconnected genes (e.g. S->E->R), but rather from uncoupling I1FFL-NFBL conjugates in favor of a pure NFBL. We simulate only relatively small TRNs, due to limitations in computational power, and this might restrict the evolutionary trajectories that are capable of generating network motifs. If simulation algorithms that scaled better with TRN size were devised, it would be interesting to explore whether network motifs would evolve via different trajectories in larger TRNs. For example, the use of the same TF for multiple regulatory purposes in real-world TRNs, which of course are larger, can constrain network evolution, requiring complex trajectories to achieve a new regulatory function (Sorrells et al. 2015).

We predicted via simulations that a highly expressed effector should promote the evolution of NFBLs over I1FFLs. Strikingly, this prediction was borne out in empirical data from yeast. A

692 highly expressed TF can more strongly regulate its target, and/or reduce the amount of noise
693 propagated downstream (Pedraza and van Oudenaarden 2005; Jothi et al. 2009). Once a highly
694 expressed TF gains a TFBS in the target gene, the TFBS may also be easier to retain during
695 evolution. Many studies on TRNs have noted a systematic difference among the expression
696 levels of genes at topologically different positions (Herrgård et al. 2003; Yu et al. 2003; Jothi et
697 al. 2009; Gerstein et al. 2012), and that highly expressed TFs are often regulators of multiple
698 target genes (Jothi et al. 2009; Gerstein et al. 2012). Our findings also support the idea that the
699 observed network motifs in TRNs are partially shaped by the expression levels of TFs.
700

701 **References**

702 Adler M, Mayo A, Alon U. 2014. Logarithmic and Power Law Input-Output Relations in Sensory Systems
703 with Fold-Change Detection. PLOS Computational Biology 10(8):e1003781.
704 Alon U. 2007. Network motifs: theory and experimental approaches. Nature Reviews Genetics 8(6):450-
705 461.
706 Amit I, Citri A, Shay T, Lu Y, Katz M et al. . 2007. A module of negative feedback regulators defines
707 growth factor signaling. Nature Genetics 39(4):503-512.
708 Artzy-Randrup Y, Fleishman SJ, Ben-Tal N, Stone L. 2004. Comment on "Network Motifs: Simple Building
709 Blocks of Complex Networks" and "Superfamilies of Evolved and Designed Networks". Science
710 305(5687):1107.
711 Balakrishnan R, Park J, Karra K, Hitz BC, Binkley G et al. . 2012. YeastMine—an integrated data
712 warehouse for *Saccharomyces cerevisiae* data as a multipurpose tool-kit. Database:bar062.

713 Basu S, Mehreja R, Thiberge S, Chen M-T, Weiss R. 2004. Spatiotemporal control of gene expression with
714 pulse-generating networks. Proceedings of the National Academy of Sciences 101(17):6355-
715 6360.
716 Brown CR, Mao C, Falkovskaia E, Jurica MS, Boeger H. 2013. Linking Stochastic Fluctuations in Chromatin
717 Structure and Gene Expression. PLoS Biology 11(8):e1001621.
718 Buzi G, Khammash M. 2016. Implementation Considerations, Not Topological Differences, Are the Main
719 Determinants of Noise Suppression Properties in Feedback and Incoherent Feedforward Circuits.
720 PLOS Computational Biology 12(6):e1004958.
721 Çağatay T, Turcotte M, Elowitz MB, Garcia-Ojalvo J, Süel GM. 2009. Architecture-Dependent Noise
722 Discriminates Functionally Analogous Differentiation Circuits. Cell 139(3):512-522.
723 Camas FM, Blázquez J, Poyatos JF. 2006. Autogenous and nonautogenous control of response in a
724 genetic network. Proceedings of the National Academy of Sciences 103(34):12718-12723.
725 Carroll SB. 2008. Evo-devo and an expanding evolutionary synthesis: a genetic theory of morphological
726 evolution. Cell 134(1):25-36.
727 Courey AJ, Jia S. 2001. Transcriptional repression: the long and the short of it. Genes & Development
728 15:2786-2796.
729 Craig R, Cortens JP, Beavis RC. 2004. Open source system for analyzing, validating, and storing protein
730 identification data. J Proteome Res 3(6):1234-42.
731 Decker KB, Hinton DM. 2013. Transcription Regulation at the Core: Similarities Among Bacterial,
732 Archaeal, and Eukaryotic RNA Polymerases. Annu. Rev. Microbiol 67:113-139.
733 Desiere F, Deutsch EW, King NL, Nesvizhskii AI, Mallick P et al. . 2006. The PeptideAtlas project. Nucleic
734 Acids Res 34(Database issue):D655-8.
735 Ferrell JE. 2016. Perfect and Near-Perfect Adaptation in Cell Signaling. Cell Systems 2(2):62-67.

736 Gancedo C, Flores C-L. 2008. Moonlighting proteins in yeasts. Microbiology and Molecular Biology
737 Reviews 72(1):197-210.
738 Gasch AP, Spellman PT, Kao CM, Carmel-Harel O, Eisen MB et al. . 2000. Genomic expression programs
739 in the response of yeast cells to environmental changes. Mol Biol Cell 11(12):4241-57.
740 Gerstein MB, Kundaje A, Hariharan M, Landt SG, Yan K-K et al. . 2012. Architecture of the human
741 regulatory network derived from ENCODE data ENCODE Encyclopedia of DNA Elements. Nature
742 488.
743 Ghaemmaghami S, Huh W-K, Bower K, Howson RW, Belle A et al. . 2003. Global analysis of protein
744 expression in yeast. Nature 425(6959):737-741.
745 Gillespie DT. 1977. Exact stochastic simulation of coupled chemical reactions. Journal of Physical
746 Chemistry 81(25):2340-2361.
747 Gomez K, Bertram J, Masel J. 2020. Mutation bias can shape adaptation in large asexual populations
748 experiencing clonal interference. Proceedings of the Royal Society B: Biological Sciences
749 287(1937):20201503.
750 Gould SJ, Lewontin RC. 1979. The Spandrels of San Marco and the Panglossian Paradigm: A Critique of
751 the Adaptationist Programme. Proceedings of the Royal Society of London. Series B, Biological
752 Sciences 205(1161):581-598.
753 Haldane JBS. 1927. A Mathematical Theory of Natural and Artificial Selection, Part V: Selection and
754 Mutation. Mathematical Proceedings of the Cambridge Philosophical Society 23(7):838-844.
755 Herrgård MJ, Covert MW, Palsson BØ. 2003. Reconciling gene expression data with known genome-scale
756 regulatory network structures. Genome research 13(11):2423-34.
757 Jenkins D, Stekel D. 2010. De Novo Evolution of Complex, Global and Hierarchical Gene Regulatory
758 Mechanisms. Journal of Molecular Evolution 71(2):128-140.

759 Jothi R, Balaji S, Wuster A, Grochow JA, Gsponer J et al. . 2009. Genomic analysis reveals a tight link
760 between transcription factor dynamics and regulatory network architecture. Mol Syst Biol 5:294.
761 Katan-Khaykovich Y, Struhl K. 2002. Dynamics of global histone acetylation and deacetylation in vivo:
762 rapid restoration of normal histone acetylation status upon removal of activators and
763 repressors. Genes & development 16(6):743-52.
764 Knabe JF, Nehaniv CL, Schilstra MJ. 2008. Do motifs reflect evolved function?—No convergent evolution
765 of genetic regulatory network subgraph topologies. Biosystems 94(1):68-74.
766 Kuo PD, Banzhaf W, Leier A. 2006. Network topology and the evolution of dynamics in an artificial
767 genetic regulatory network model created by whole genome duplication and divergence.
768 BioSystems 85:177-200.
769 Lee TI, Rinaldi NJ, Robert F, Odom DT, Bar-Joseph Z et al. . 2002. Transcriptional regulatory networks in
770 Saccharomyces cerevisiae. science 298(5594):799-804.
771 Lynch M. 2007. The evolution of genetic networks by non-adaptive processes. Nature Reviews Genetics
772 8(10):803-813.
773 Mangan S, Alon U. 2003. Structure and function of the feed-forward loop network motif. Proc Natl Acad
774 Sci U S A 100(21):11980-5.
775 Mao C, Brown CR, Falkovskaia E, Dong S, Hrabeta-Robinson E et al. . 2010. Quantitative analysis of the
776 transcription control mechanism. Molecular Systems Biology 6:431.
777 Mazurie A, Bottani S, Vergassola M. 2005. An evolutionary and functional assessment of regulatory
778 network motifs. Genome Biology 6(4):R35.
779 Milo R, Shen-Orr S, Itzkovitz S, Kashtan N, Chklovskii D et al. . 2002. Network motifs: simple building
780 blocks of complex networks. Science 298(5594):824-7.
781 Payne JL, Wagner A. 2015. Function does not follow form in gene regulatory circuits. Scientific Reports
782 5:13015.

783 Pedraza JM, van Oudenaarden A. 2005. Noise Propagation in Gene Networks. Science 307(5717):1965-
784 1969.
785 Poss ZC, Ebmeier CC, Taatjes DJ. 2013. The Mediator complex and transcription regulation. Critical
786 Reviews in Biochemistry and Molecular Biology 48(6):575-608.
787 Rosenfeld N, Elowitz MB, Alon U. 2002. Negative Autoregulation Speeds the Response Times of
788 Transcription Networks. Journal of Molecular Biology 323(5):785-793.
789 Ruths T, Nakhleh L. 2013. Neutral forces acting on intragenomic variability shape the *Escherichia coli*
790 regulatory network topology. Proceedings of the National Academy of Sciences of the United
791 States of America 110(19):7754-7759.
792 Shen-Orr SS, Milo R, Mangan S, Alon U. 2002. Network motifs in the transcriptional regulation network
793 of *Escherichia coli*. Nat Genet 31(1):64-8.
794 Shi W, Ma W, Xiong L, Zhang M, Tang C. 2017. Adaptation with transcriptional regulation. Scientific
795 Reports 7(1):42648.
796 Shoval O, Alon U. 2010. SnapShot: Network Motifs. Cell 143(2):326-326.e1.
797 Shoval O, Goentoro L, Hart Y, Mayo A, Sontag E et al. . 2010. Fold-change detection and scalar symmetry
798 of sensory input fields. Proceedings of the National Academy of Sciences 107(36):15995-16000.
799 Solé RV, Valverde S. 2006. Are network motifs the spandrels of cellular complexity? Trends in Ecology &
800 Evolution 21(8):419-422.
801 Sorrells TR, Booth LN, Tuch BB, Johnson AD. 2015. Intersecting transcription networks constrain gene
802 regulatory evolution. Nature 523(7560):361-365.
803 Sorrells TR, Johnson AD. 2015. Making Sense of Transcription Networks. Cell 161:714-723.
804 Stern DL, Orgogozo V. 2009. Is genetic evolution predictable? Science 323(5915):746-751.
805 Stoltzfus A, McCandlish DM. 2017. Mutational Biases Influence Parallel Adaptation. Molecular Biology
806 and Evolution 34(9):2163-2172.

807 Teixeira MC, Monteiro P, Jain P, Tenreiro S, Fernandes AR et al. . 2006. The YEASTRACT database: a tool
808 for the analysis of transcription regulatory associations in *Saccharomyces cerevisiae*. Nucl. Acids
809 Res. 34(suppl_1):D446-451.
810 Tsuda ME, Kawata M. 2010. Evolution of Gene Regulatory Networks by Fluctuating Selection and
811 Intrinsic Constraints. PLoS Comput Biol 6(8):e1000873.
812 van Nimwegen E, Crutchfield JP. 2000. Metastable evolutionary dynamics: crossing fitness barriers or
813 escaping via neutral paths? Bull Math Biol 62(5):799-848.
814 Wagner A. 2003. Does Selection Mold Molecular Networks? Sci. STKE 2003(202):pe41.
815 Wall ME, Hlavacek WS, Savageau MA. 2004. Design of gene circuits: lessons from bacteria. Nature
816 Reviews Genetics 5(1):34-42.
817 Wang E, Purisima E. 2005. Network motifs are enriched with transcription factors whose transcripts
818 have short half-lives. Trends Genet 21(9):492-495.
819 Wang M, Herrmann CJ, Simonovic M, Szklarczyk D, von Mering C. 2015. Version 4.0 of PaxDb: Protein
820 abundance data, integrated across model organisms, tissues, and cell-lines. Proteomics
821 15(18):3163-3168.
822 Whitlock MC, Phillips PC, Moore FB-G, Tonsor SJ. 1995. MULTIPLE FITNESS PEAKS AND EPISTASIS. Annual
823 Review of Ecology and Systematics 26(1):601-629.
824 Widder S, Solé R, Macía J. 2012. Evolvability of feed-forward loop architecture biases its abundance in
825 transcription networks. BMC Systems Biology 6(1):7.
826 Xiong K, Lancaster AK, Siegal ML, Masel J. 2019. Feed-forward regulation adaptively evolves via
827 dynamics rather than topology when there is intrinsic noise. Nature Communications
828 10(1):2418.
829 Yampolsky LY, Stoltzfus A. 2001. Bias in the introduction of variation as an orienting factor in evolution.
830 Evolution and Development 3(2):73-83.

831 Yu H, Luscombe NM, Qian J, Gerstein M. 2003. Genomic analysis of gene expression relationships in

832 transcriptional regulatory networks. Trends in Genetics 19(8):422-427.

833

834 **Acknowledgement**

835 We acknowledge the generous computational resources provided by the High Performance

836 Computation Center of the University of Arizona.

837

838 **Funding**

839 This work is supported by funding from the USA NSF Award awarded to MG.

840

841 **Conflicts of Interest**

842 The authors declare no conflict of interest.

Supplementary materials

Table S1. Major model parameters[1]

Parameter	Values[2]	Bounds[3]	References
Length of cis-regulatory sequence	150 bp		(Yuan et al. 2005)
Length of TF recognition sequence	8 bp		(Wunderlich and Mirny 2009)
Length occupied by a TF on each side of recognition sequence	3 bp		(Zhu and Zhang 1999)
Dissociation constant between TF and perfect TFBS, $K_d(0)$	**$10^{U(-9,-6)}$ mole per liter**[4]	$(0, 10^{-5})$	(Park et al. 2004; Nalefski et al. 2006)
Dissociation constant between TF and non-specific DNA, $K_d(3)$	10^{-5} M		(Maerkl and Quake 2007)
Base rate of transition from Repressed to Intermediate	0.15 min^{-1}		(Katan-Khaykovich and Struhl 2002)
Maximum transition rate from Repressed to Intermediate	0.92 min^{-1}		(Katan-Khaykovich and Struhl 2002; Brown et al. 2013)
Base rate of transition from Intermediate to Repressed	0.67 min^{-1}		(Katan-Khaykovich and Struhl 2002)
Maximum transition rate from Intermediate to Repressed	4.11 min^{-1}		Chosen to give same dynamic range and Repressed to Intermediate
Base rate of transition from Intermediate to Active	0.025 min^{-1}		(Brown et al. 2013)
Maximum transition rate from Intermediate to Active	3.3 min^{-1}		(Brown et al. 2013)
Transition rate from Active to Intermediate, $r_{Act\_to\_Int}$	**$10^{N(1.27, 0.226)}$ min^{-1}**[4]	[0.59, 64.7]	(Guillemette et al. 2005; Pelechano et al. 2010; Brown et al. 2013)
Length of gene, L	**$10^{N(2.568, 0.34)}$ codons**	[50, 5000]	(SGD Project) (Balakrishnan et al. 2012)
Rate of transcription initiation, $r_{max\_transc\_init}$	6.75 min^{-1}		(Brown et al. 2013)
Speed of transcription elongation	600 codon min^{-1}		(Dujon 1996; Larson et al. 2011; Hocine et al. 2013)
Time for transcribing UTRs and for terminating transcription	1 min		(Dujon 1996; Larson et al. 2011; Hocine et al. 2013)
Rate of mRNA degradation, r_{mRNA_deg}	**$10^{N(-1.49, 0.267)}$ min^{-1}**	$[7.5\times10^{-4}, 0.54]$	(Wang et al. 2002)
Speed of translation elongation	330 codon min^{-1}		(Siwiak et al. 2010)
Translation initiation time	0.5 min		(Siwiak et al. 2010)
Protein synthesis rate, $r_{protein\_syn}$	**$10^{N(0.322, 0.416)}$ molecule $mRNA^{-1}$ min^{-1}**	$[4.5\times10^{-3}, 61.4]$	(Siwiak et al. 2010)
Rate of protein degradation, $r_{protein\_deg}$	**$10^{N(-1.88, 0.561)}$ min^{-1}**	$[3.0\times10^{-6}, 0.69]$	(Belle et al. 2006)
Saturation concentration of effector protein, N_{e_sat}	10,000 molecules $cell^{-1}$		(Ghaemmaghami et al. 2003)
Fitness cost of protein expression for a gene with $L = 10^{2.568}$, c_{transl}	2×10^{-6} $molecules^{-1}$ min^{-1}		(Ghaemmaghami et al. 2003; Kafri et al. 2016)
Maximum number of effector gene copies	5		
Maximum number of TF gene copies, excluding the signal	19		

[1] This table is reproduced without modification from Xiong et al. (2019) under a Creative Commons Attribution 4.0 International License (https://creativecommons.org/licenses/by/4.0/).

[2] Parameters in bold can be altered by mutation, and the table shows the distributions from which their initial values are sampled. Estimation of N_{e_sat} is described in the Methods; estimation of the other parameters is described in the Supplementary Methods.

[3] Same units as the parameter values. Parentheses mean the parameter cannot take the boundary values; square brackets mean it can. We also use these bounds to constrain mutation (see Supplementary Methods).

[4] The uniform distribution is denoted U(min, max).

[5] The normal distribution is denoted N(mean, SD).

Table S2. Mutation rates and effect sizes[1]

Mutation	Relative rate	Effect of mutation[2]
Single nucleotide substitution	5.25×10^{-8} per gene	
Gene deletion	1.5×10^{-7} per gene[3]	
Gene duplication	1.5×10^{-7} per gene[3]	
Mutation to consensus sequence of a TF	3.5×10^{-9} per gene	
Mutation to TF identity (activator vs. repressor)	3.5×10^{-9} per gene	
Mutation to $K_d(0)$	3.5×10^{-9} per gene	$k = 0.5$, $\mu = -5$[3], $\sigma = 0.776$
Mutation to L	1.2×10^{-11} per codon	
Mutation to $r_{protein\_syn}$	9.5×10^{-12} per codon	$k = 0.5$, $\mu = 0.021$[3], $\sigma = 0.760$

Mutation to $r_{protein\_deg}$	9.5×10^{-12} per codon	k = 0.5, μ = -1.88, σ = 0.739
Mutation to $r_{Act\_to\_Int}$	9.5×10^{-12} per codon	k = 0.5, μ = 1.57[3], σ = 0.773
Mutation to r_{mRNA_deg}	9.5×10^{-12} per codon	k = 0.5, μ = -1.19, σ = 0.396

[1] This table is reproduced without modification from Xiong et al. (2019) under a Creative Commons Attribution 4.0 International License (https://creativecommons.org/licenses/by/4.0/).

[2] Mutation to these quantitative rates takes the form $\log_{10}x' = \log_{10}x + \mathrm{Normal}(k(\mu - \log_{10}x), \sigma)$, where x is the original value of the rate and x' is the value after mutation. See Supplementary Methods for details.

[3] The value of this parameter is different during burn-in. See Supplementary Methods for details.

Optimal peak		Initial condition 25		Initial condition 31		Initial condition 79	
		Evo. step 1 - 10,000	Evo. step 10,001 – 20,000	Evo. step 1 - 5,000	Evo. step 5,001 – 10,000	Evo. step 1 - 10,000	Evo. step 10,001 – 20,000
Low	I1FFL-creating	0.050	0.217	0.680	0.067	0.051	0.586
	NFBL-creating	0.107	0.007	0.006	0.003	0.106	0.013
Medium	I1FFL-creating	0.065	0.075	0.811	0.365	0.105	0.047
	NFBL-creating	0.111	0.104	0.016	0.025	0.112	0.171
High	I1FFL-creating	0.013	0.034	0.875	0.059	0.048	0.118
	NFBL-creating	0.729	0.413	0.007	0.201	0.259	0.174

Table S3. Mutational bias toward particular motifs can shift over the course of evolution. We focus our analysis on three random TRN initializations (conditions 25, 31, and 79) that evolved to high fitness in all three selection conditions. Under selection for high peak effector expression, all three simulations evolved NFBLs (i.e. the occurrence of NFBL > 0.5 and the occurrence of I1FFL < 0.5). Under selection for low or medium effector expression, all three evolved I1FFLs. As in Table 1, we show the number of mutations normalized by the total number of mutations trialed in resident TRNs that did not contain the motif in question. As an example of a change in mutational bias, initial condition 25 under selection for low peak effector expression initially creates NFBLs more often but later creates I1FFLs more often.

peak level		Evolutionary step 1 – 10,000		Evolutionary step 10,001 – 30,000	
		Trialed	Acceptance rate	Trialed	Acceptance rate
Low	I1FFL-destroying	0.100	0.072	0.065	0.051
	NFBL-destroying	0.141	0.139	0.196	0.128
Medium	I1FFL-destroying	0.129	0.068	0.087	0.069
	NFBL-destroying	0.157	0.108	0.125	0.108
High	I1FFL-destroying	0.117	0.074	0.114	0.057
	NFBL-destroying	0.086	0.120	0.063	0.124

Table S4. Summary of mutations that remove all I1FFLs and/or NFBLs. For each selection condition, we pooled qualified mutations from all high-fitness replicates shown in Fig. 2. A mutation is classed as destroying if it eliminates all instances of the given motif. The total number of qualified mutations were

normalized by the total number of mutations trialed in resident TRNs that contained the motif of interest. The acceptance rate is the number of accepted mutations across all replicates divided by the number of trialed mutations across all replicates.

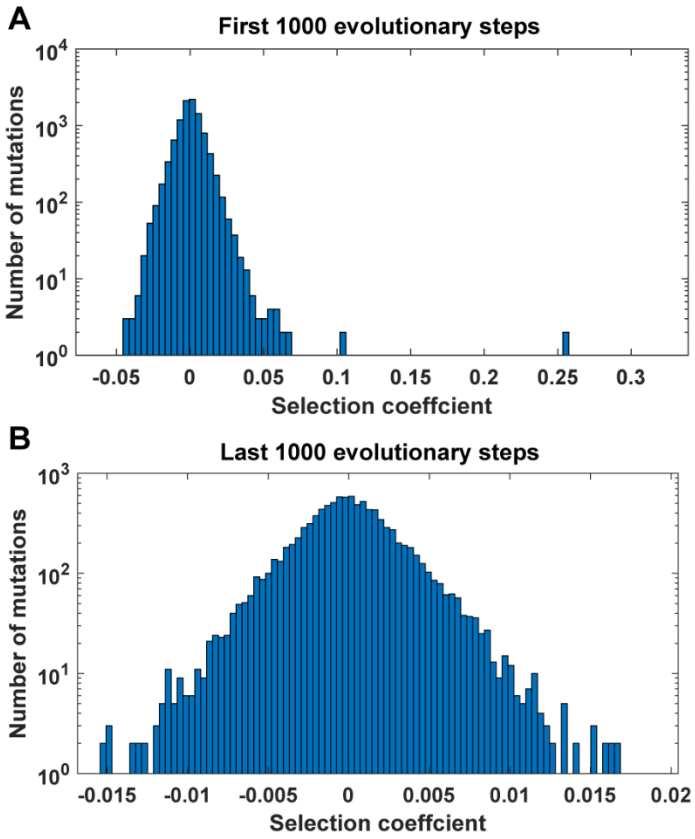

Figure S1. Evolutionary paths include slightly deleterious mutations. We pooled all accepted mutations from 10 evolutionary simulations under selection for high peak effector expression. Selection coefficients were calculated from the average fitness across 1,000 simulations of gene expression. Note while fitness is therefore biased by the 200 replicates used to decide to accept that mutation, this bias applies to both resident and mutant. We measure noise on top of the true distribution of fitness effects, suggesting that the underlying distribution is narrower than shown here. **(A)** Data restricted to the first 1,000 evolutionary steps, during which fitness generally increases rapidly. (**B**) Data restricted to the last 1,000 evolutionary steps, during which almost all simulations have reached a fitness plateau.

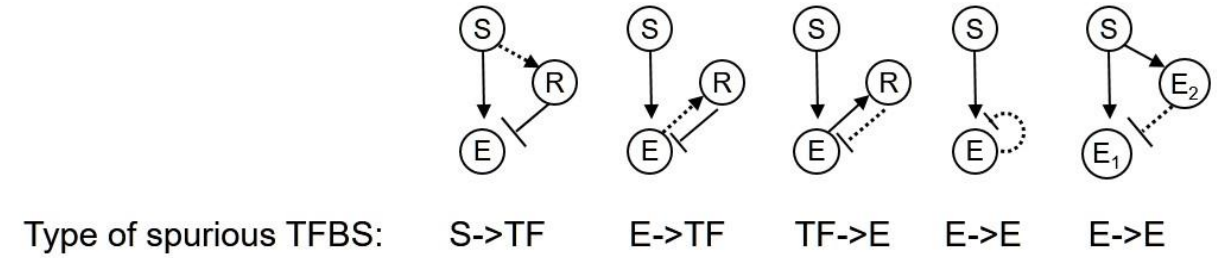

Figure S2. Five scenarios in which apparent but non-functional network motifs can arise from spurious TFBSs. A TFBS containing 2 mismatches can easily appear by chance in a cis-regulatory sequence, but may be deemed spurious if it has negligible functional effect. Spurious E->E TFBSs where both "Es" represent the same effector gene give rise to apparent ARs, whereas if they represent different effector proteins, they give rise to I1FFLs.

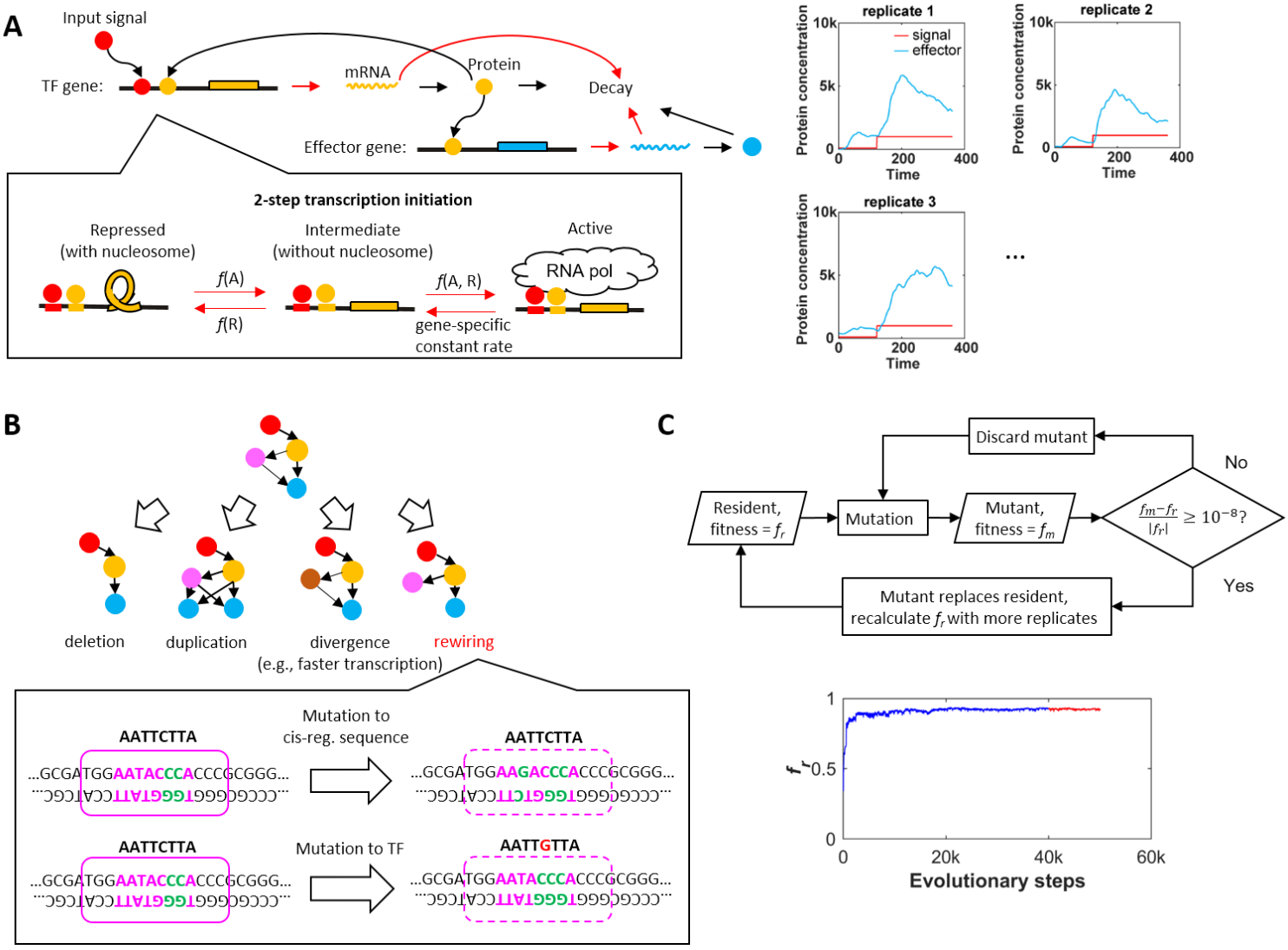

Figure S3. Summary of the model. (A) Simulation of gene expression in a TRN that has two TF genes, one of which is the effector (cyan). Here the input signal, which is simulated as an activator, binds to the cis-regulatory sequence of the non-effector TF gene (TF binding is demonstrated in **(B)**) and induces gene expression. Transcription initiation is a two-step process where most of the transition rates are functions of the concentrations of activators and/or repressors (see Transcriptional regulation in the supplement). Biological processes marked by red arrow are simulated as stochastic processes, and those marked by black arrows are simulated by solving ordinary differential equations (see Simulation of gene expression in the supplement). We use the expression levels of the effector in response to a two-stage input signal to calculate the fitness (see Methods for details). The simulation of gene expression is repeated and the average fitness of the replicates is used as the fitness of the TRN (see Methods for details). The diagram of transcription and translation is revised from Xiong et al. (2019) under a Creative Commons Attribution 4.0 International License (https://creativecommons.org/licenses/by/4.0/). **(B)** A TRN goes through one of many types of mutation (see Model Overview for details) that change the size of the network, rewire the network, or change one property of a gene in the network. The zoom-in depicts turnover of TF binding sites, which can rewire the network. The purple box represents the TF

and on top of the box is the consensus binding sequence of the TF. At most two mismatches (green letters) to the consensus binding sequences can be tolerated. Point mutations in the cis-regulatory sequence of the target gene and in the consensus binding sequence of the TF can increase mismatch, causing the loss of a TF binding site. Note that the TF occupies additional sequences when binds to the DNA. **(C)** Evolution of TRNs is simulated as an origin-fixation process. Evolution starts with a random TRN, which is called the resident. if the mutant's fitness is sufficiently high (see Methods for details), it replaces the resident and becomes the new resident (see Methods for details), which is defined as one evolutionary step. Otherwise, new mutants are generated until the replacement happens. The evolution is simulated for 50,000 evolutionary steps, which is generally long enough for the resident's fitness to reach a plateau.

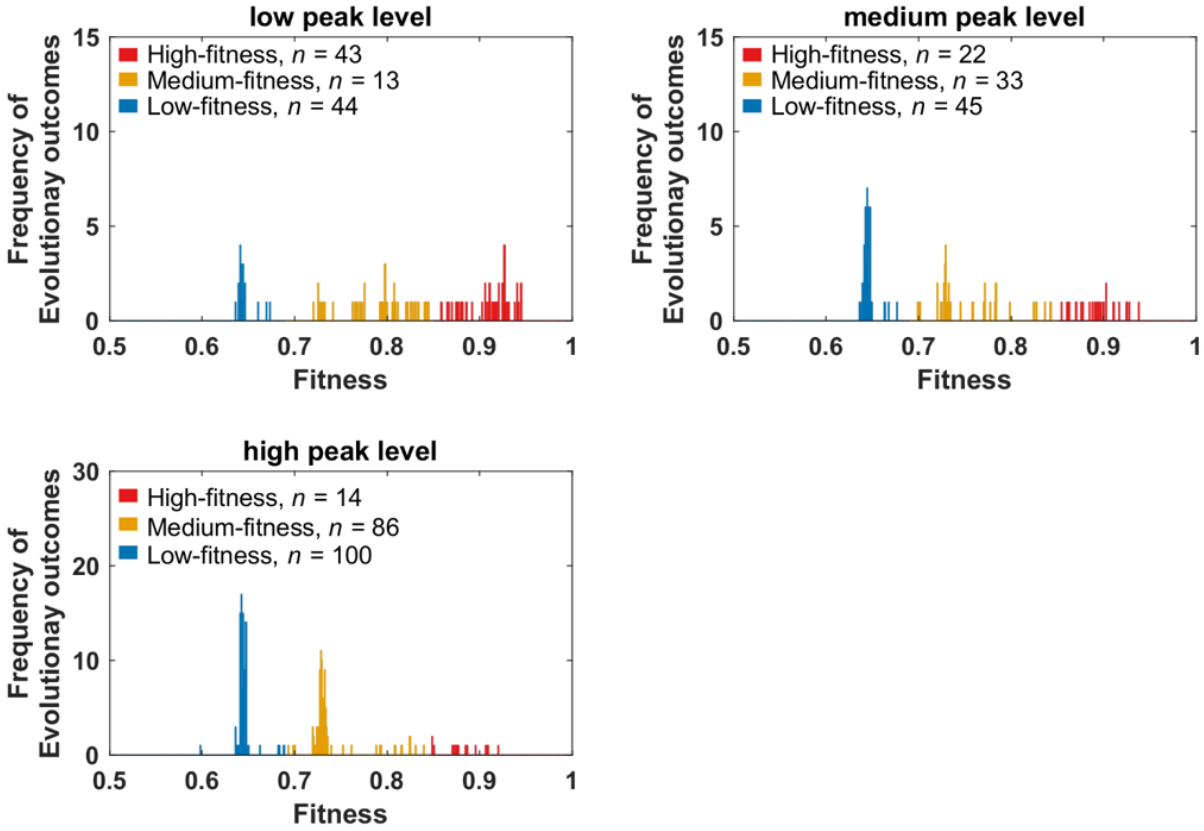

Figure S4. Fitness distributions of genotypes evolved with different optimal peak levels of the effector. We ran 100 evolutionary simulations for the low-peak and the medium-peak conditions, and 200 for the high-peak condition. For each simulation, we calculate the fitness of the evolved genotype as the average fitness of the last 10,000 evolutionary steps. For all three selection conditions, genotypes with fitness above 0.845 are considered as high-fitness genotypes and are further analyzed in **Fig. 2**. We used a fitness cutoff of 0.69 to separate medium-fitness genotypes and low-fitness genotypes.

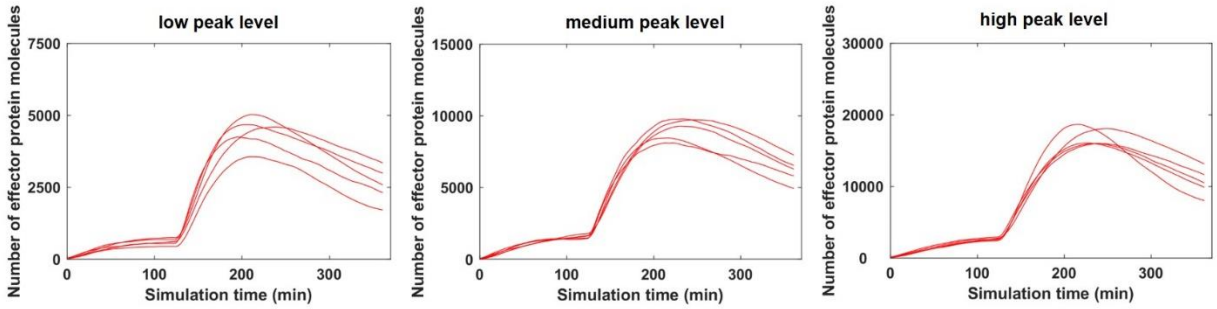

Figure S5. Phenotype of high-fitness replicates. For each selection condition, we randomly picked 5 high-fitness replicates from those defined in Fig. S4. We ran 200 simulations to characterize the expression profile of the effector, as found at evolutionary step 50,000 in each replicate. Each trajectory shows the expression levels of the effector averaged across the 200 simulations, and starts after the burn-in of gene expression (see **Methods** for details).

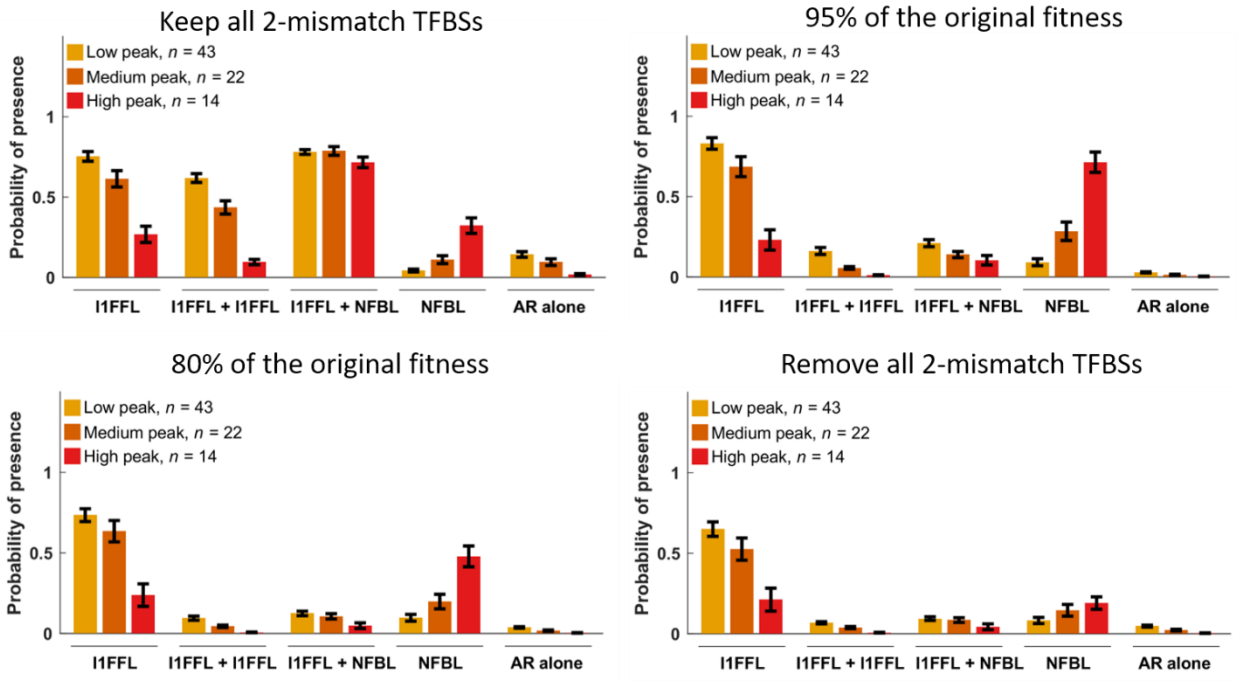

Figure S6. The relative occurrences of motifs do not depend strongly on the criteria for removing spurious 2-mismatch TFBSs. Results are from the same high-fitness evolutionary replicates shown in Fig. 2A, where sets of TFBSs were excluded when their removal yielded fitness of at least 99% of the fitness observed in their presence. Data are shown as mean ± SE over replicates.

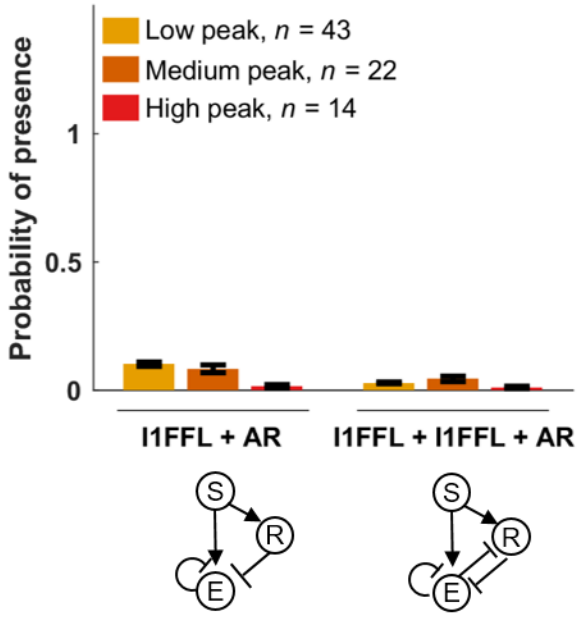

Figure S7. Auto-repression (AR) rarely evolves with I1FFLs or overlapping I1FFLs. In high-fitness genotypes evolved under selection for pulse generation, there were few auto-repressing effectors co-occurring with other motifs, and for simplicity, they were therefore grouped in **Fig. 2** with the motif with which they co-occurred. We note that when the repressor of an I1FFL-NFBL conjugate is an effector, this effector can form auto-repression. We classified such case as a stand-alone AR, because from the perspective of this effector, it is not regulated by an I1FFL, NFBL, overlapping I1FFL, or I1FFL-NFBL conjugate. Data are shown as mean ± SE over replicates.

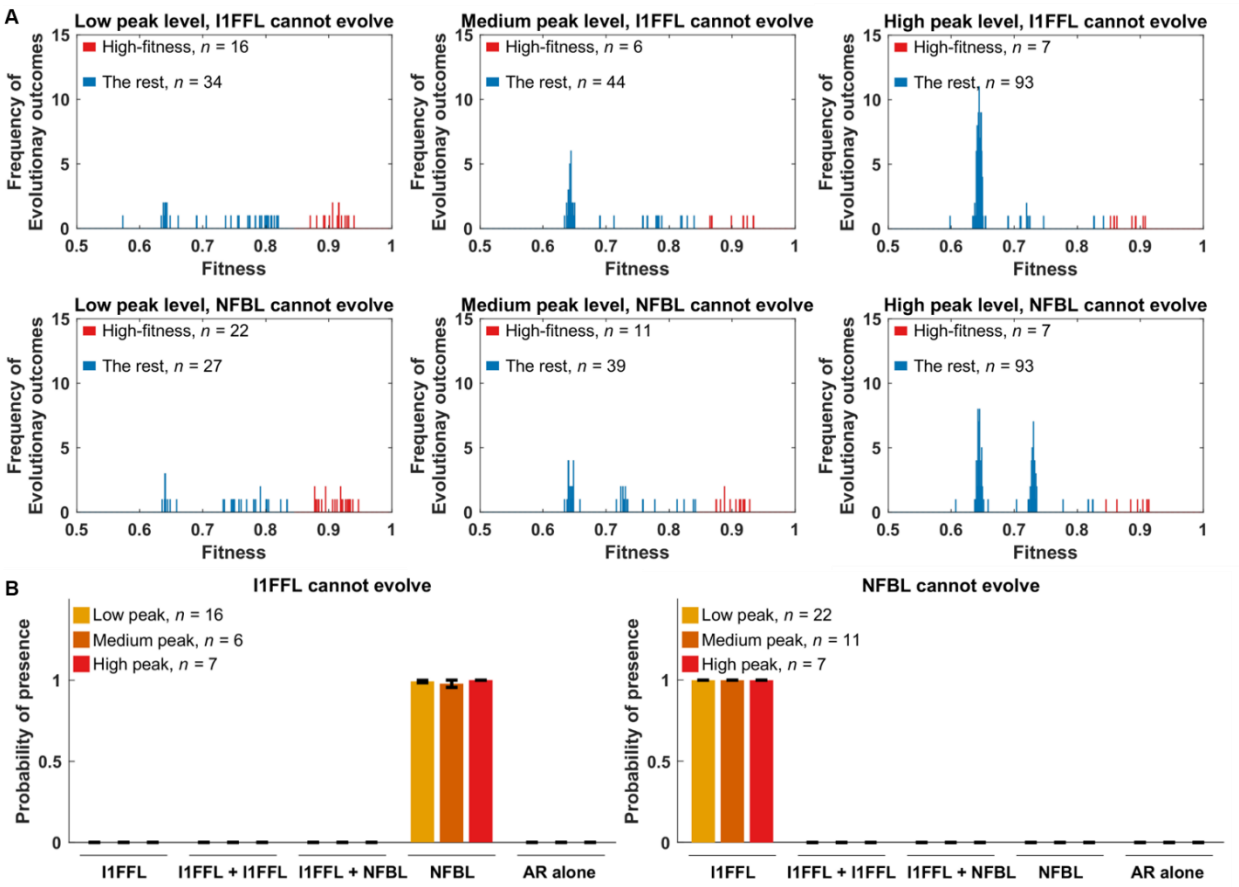

Figure S8. Fitness distributions and network occurrences of genotypes with restricted solutions under different selection conditions. (A) Each panel under low peak and medium peak selection summarized 50 evolutionary simulations, and the two panels under high peak each summarize 100 evolution simulations. Under the condition where we select for a low peak and prevent NFBLs from evolving, we removed one simulation that was terminated prematurely before evolving 50,000 evolutionary steps. This particular simulation failed to find a mutant that has higher fitness than the resident phenotype even after 2,000 trials. To classify a genotype as high-fitness (red), we apply the same fitness cutoff as in **Fig. S1**. The average fitness of the high-fitness genotypes is shown in **Fig. 3B**. See legend of **Fig. 2B** for description of modifications to prevent the evolution of NFBLs or I1FFLs. **(B)** In the high-fitness genotypes, when either I1FFL or NFBL is not allowed to evolve, the other motif almost always evolves. Data are shown as mean ± SE over replicates.

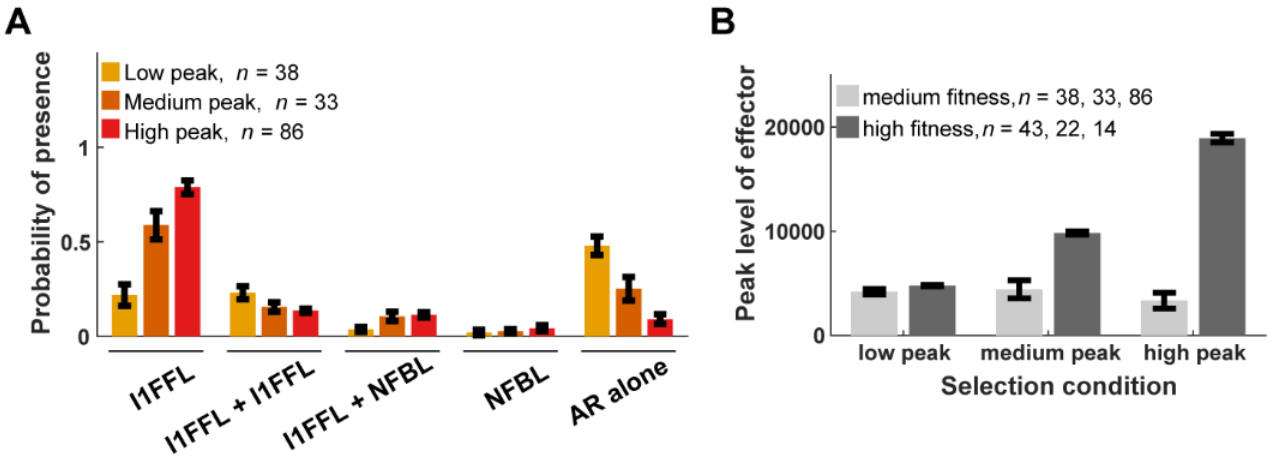

973 **Figure S9. Medium-fitness genotypes fail to achieve high peak effector expression, and primarily**
974 **evolve I1FFLs and auto-repression. (A)** Methods are the same as for **Fig. 2A**, applied here to medium-
975 fitness evolutionary replicates. **(B)** For each high-fitness and medium-fitness replicate shown in Fig. S4,
976 we average the peak protein levels of the effector over 200 replicate simulations of gene expression.
977 Data are shown as mean ± SE over replicates.
978

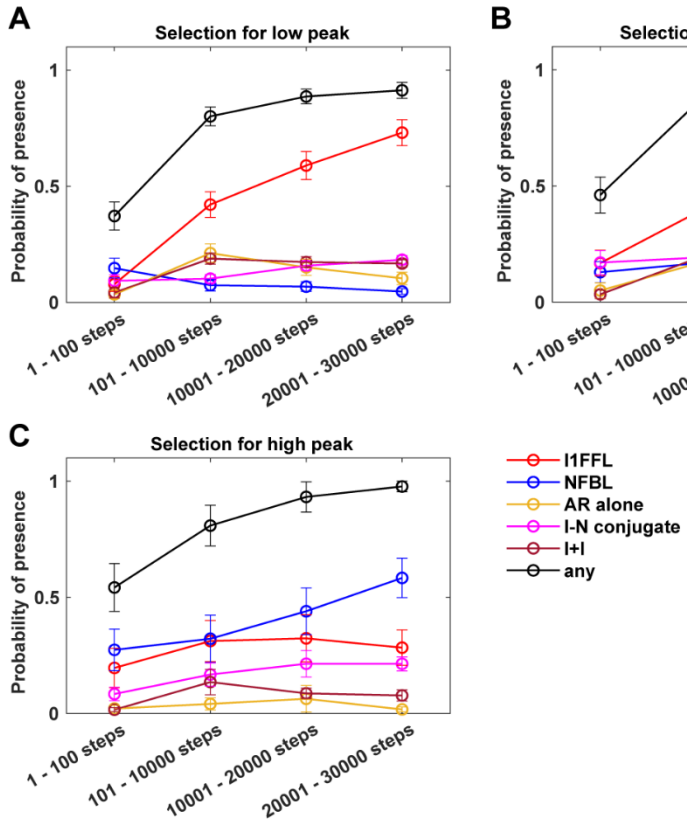

979 **Figure S10. The occurrence of all motifs during evolution.** We calculated the proportion of evolutionary
980 steps that contain at least one motif of that type. Details are the same as for **Fig. 3**, except here we show
981 a broader range of motifs as shown in **Fig. 2**. Data are shown as mean ± SE over the high-fitness
982 replicates.
983

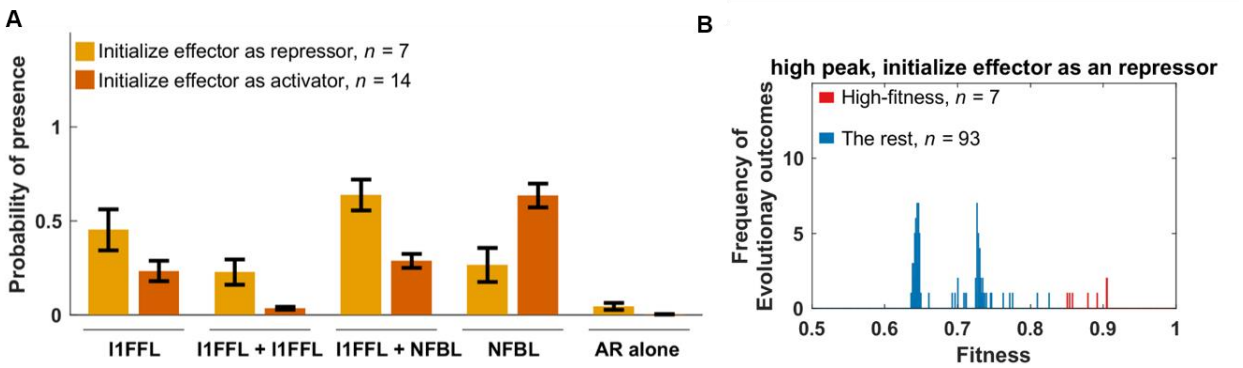

Figure S11. Initializing the effector as a repressor facilitates the evolution of I1FFLs. We repeated evolution under selection for high peak effector expression, but initialized the effector as a repressor rather than as an activator. **(A)** Motif occurrence compared to the activator-initialized evolutionary conditions given in **Fig. 2**. Data are shown as mean ± SE over replicates. **(B)** Fitness of the evolved TRNs. Similar to Fig. S1, TRNs with fitness of 0.845 or higher are considered high-fitness.

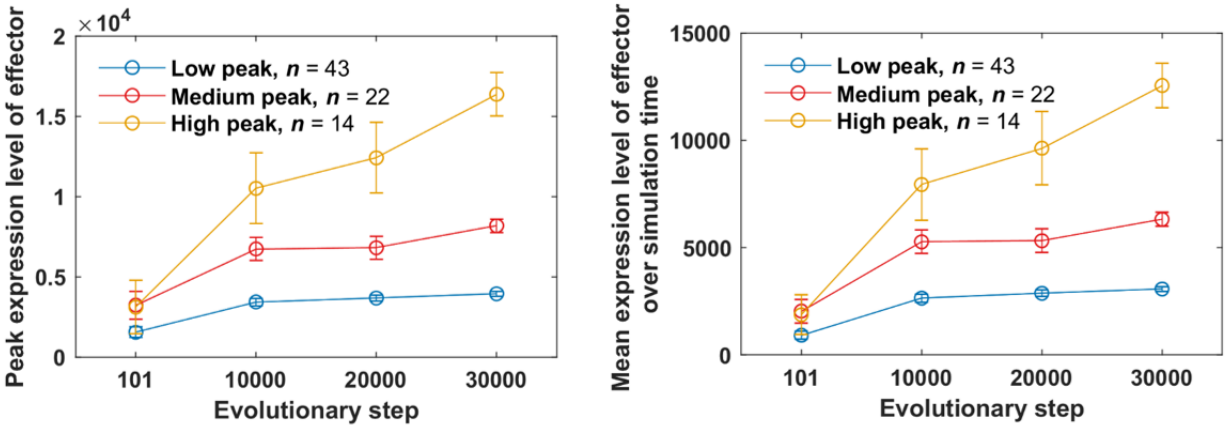

Figure S12. High peak effector expression evolves slowly. For each high-fitness replicate shown in Fig. 2A, we average the peak protein levels of the effector over 200 replicate simulations of gene expression. Data are shown as mean ± SE over replicates.

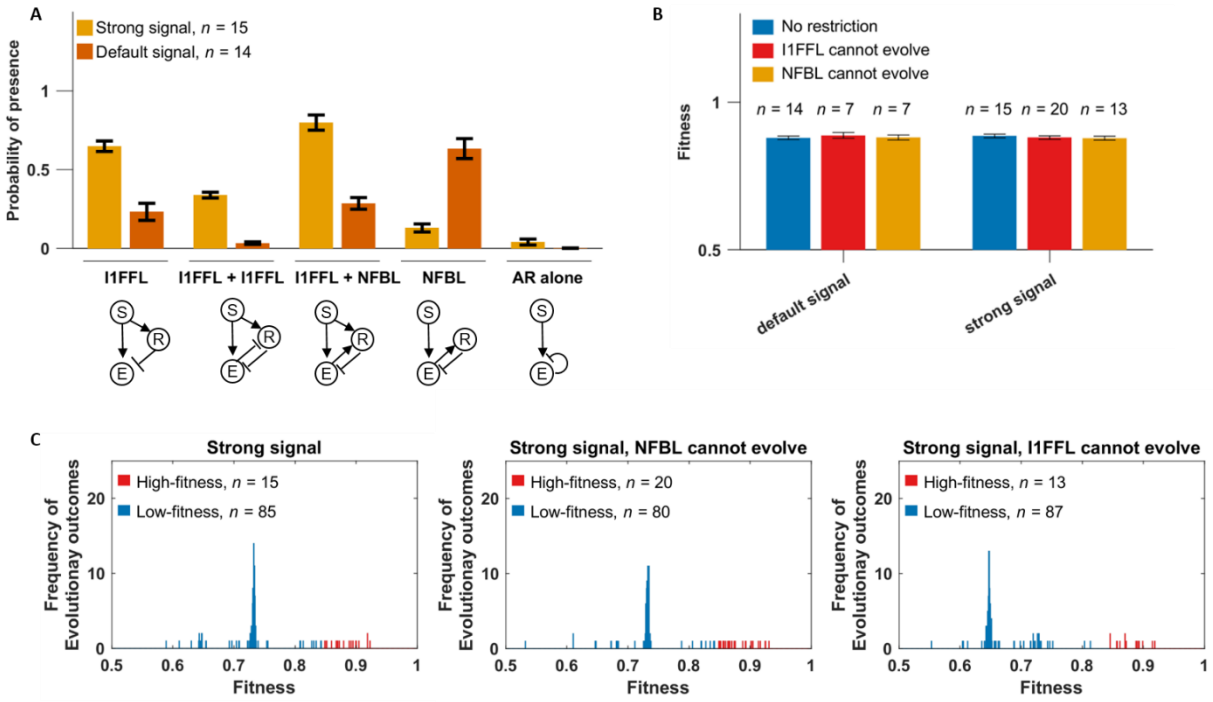

Figure S13. A stronger signal increases I1FFL prevalence. We compared evolution under the default signal, where signal strength increases from 100 molecules per cell to 1,000 molecules per cell, to a stronger signal, where the signal strength increases from 1,000 molecules per cell to 10,000 molecules per cell. **(A)** Occurrence of different motifs in high-fitness genotypes. **(B)** I1FFLs or NFBLs can yield similar fitness under a given signal regime. Data are shown as mean ± SE over replicates. **(C)** Fitness distribution of genotypes evolved with a strong signal without (leftmost) or with (middle and rightmost) restrictions on evolution. Similarly to Figs. S1 and S3, we define high-fitness genotypes to be those with fitness greater or equal to 0.845.

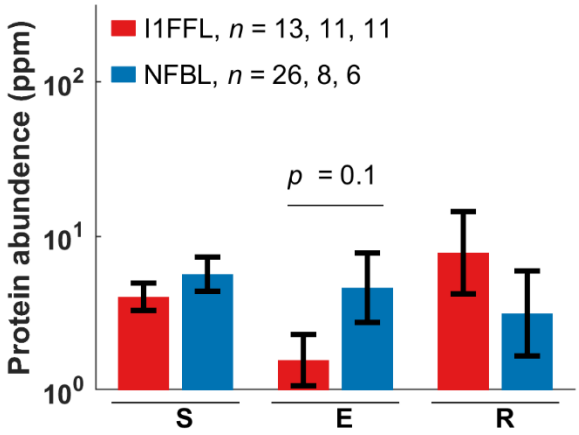

Figure S14. Effectors have higher protein expression in NFBLs than in I1FFLs in *S. cerevisiae* across a more comprehensive dataset. Protein expression levels are from the "GPM, Aug, 2014" dataset provided by PaxDB (Wang et al. 2015). Data are shown as mean ± SE (of log-transformed data in the case of protein expression) over each network position across all instances of the motif, excluding positions

where the data are not available. For each motif type, we list the numbers of genes with available expression level data at signal nodes, effector nodes, and repressor nodes. Statistical significance is assessed using two-tailed t-tests.

Details of the model

The following sections are copied from Xiong et al. (2019). Parts of the original text were rewritten or deleted for brevity. The original article was licensed under the Creative Commons Attribution 4.0 International License, which grants free copy and modification. A copy of the license can be found at https://creativecommons.org/licenses/by/4.0/.

TF binding

In our model, each gene is controlled by a 150-bp cis-regulatory region, corresponding to a typical yeast nucleosome-free region within a promoter (Yuan et al. 2005). TFBSs can evolve in the cis-regulatory region, and we set the length of a consensus binding sequence to be 8 bp. Assuming that only one of the four nucleotides is a good match at each of the 8 base pairs, then the 8-bp consensus binding sequence has an information of 16 bits, which is slightly larger than that of a typical yeast TF (13.8 bits) (Wunderlich and Mirny 2009). We assume a higher information content than seen empirically in order to reduces the number of TFBSs within the cis-regulatory regions to a point that our computational power can handle. We allow up to 2 mismatches in the consensus binding sites, based on the finding that, with up to 2 mismatches in the 6-bp binding sequence, some yeast TFs can still bind DNA at above background level (Maerkl and Quake 2007). To capture competitive binding between TFs, we assume that two TFs cannot simultaneously occupy overlapping stretches, which we assume extend beyond the recognition sequence to occupy a total of 14 bp (Zhu and Zhang 1999).

We denote the dissociation constant of a TFBS with m mismatches as $K_d(m)$. Sites with $m > 3$ mismatches are assumed to still bind at a background rate equal to $m = 3$ mismatches, with dissociation constant $K_d(3) = 10^{-5}$ mole per liter (Maerkl and Quake 2007) for all TFs. We assume that each of the last three base pairs makes an equal and independent additive contribution $\Delta G_{bp} < 0$ to the binding energy (Benos et al. 2002). We ignore cooperativity in binding. Dissociation constants of eukaryotic TFs for perfect TFBSs can range from 10^{-5} mole per liter (Park et al. 2004) to 10^{-11} mole per liter (Nalefski et al. 2006). We initialize each TF with its own value of $\log_{10}(K_d(0))$ sampled from a uniform distribution between -6 and -9, with mutation capable of further expanding this range, subject to $K_d(0) < 10^{-5}$ mole per liter. Substituting $m = 0$ and $m = 3$ into

$$\Delta G_m = -RT\ln K_{\mathrm{d}}(m) = \Delta G_0 - \min(m, 3)\Delta G_{\mathrm{bp}}, \quad (1)$$

where R is the gas constant and T is temperature, we can solve for ΔG_{bp} and ΔG_0, and thus obtain $K_d(1)$ and $K_d(2)$ (the dissociation constants for TFBS with one and two mismatches, respectively).

We rescale K_d values to effective K_d values to account for the "dilution" of TFs by non-specific TF binding sites (NSBSs) in the genome. A haploid *S. cerevisiae* genome is 12 Mb, 80% of which is wrapped in nucleosomes (Lee et al. 2007), yielding approximately 10^6 potential NSBSs. In a yeast nucleus of volume 3×10^{-15} liters, the NSBS concentration is of order 10^{-4} mole per liter. To find the concentration of free TF [TF] in the nucleus given a total nucleic TF concentration of C_{TF}, we consider

$$K_{\mathrm{d}} = \frac{[\mathrm{binding\_site}][\mathrm{TF}]}{[\mathrm{binding\_site{\cdot}TF}]}, \quad (2)$$

in the context of NSBSs, substitute [TF·NSBS] with C_{TF} - [TF], and solve for

$$[\mathrm{TF}] = \frac{K_\mathrm{d}(3)}{K_\mathrm{d}(3)+[\mathrm{NSBS}]} C_\mathrm{TF} = \frac{10^{-5}}{10^{-5}+10^{-4}} C_\mathrm{TF} \approx 0.1 C_\mathrm{TF}. \quad (3)$$

Thus, about 90% of total TFs are bound non-specifically, leaving about 10% free. The relatively small number of specific TFBSs is not enough to significantly perturb the proportion of free TFs, and so for the specific TFBSs with $m < 3$ that are of interest in our model, we simply use $\widehat{K}_\mathrm{d}(m) = 10K_\mathrm{d}(m)$ to account for the reduction in the amount of available TF due to non-specific binding. We also convert $\widehat{K}_\mathrm{d}$ from the units of mole per liter in which K_d is estimated empirically to the more convenient molecules per nucleus. The rescaling factor r for which $\widehat{K}_\mathrm{d}$ (in molecule per nucleus) = $r\widehat{K}_\mathrm{d}$ (in mole per liter) is 3×10^{-15} liter per nucleus $\times\ 6.02 \times 10^{23}$ molecule mole^{-1} = 1.8×10^{9} molecule cell^{-1} liter mole^{-1}. Taken together, $\widehat{K}_\mathrm{d}$ (molecule per nucleus) = $10rK_\mathrm{d}$ (mole per liter), where the factor 10 accounts for non-specific TF binding.

TF occupancy

Here we calculate the probability that there are *A* activators and *R* repressors bound to a given cis-regulatory region at a given moment in gene expression time. First we note that if we consider TF *i* binding to TFBS *j* in isolation from all other TFs and TFBSs, Supplementary Equation 4 gives us the probability of being bound:

$$P_\mathrm{b}(j) = 1 - P_\mathrm{u}(j) = \frac{C_i}{\widehat{K}_\mathrm{d}+C_i} \quad (4)$$

Let $P_{A,R}^{(n)}$ be a term proportional (for a given value of *n*) to the combined probability of all binding configurations in which exactly *A* activators and *R* repressors are bound to the first *n* binding sites along the cis-regulatory sequence. We calculate $P_{A,R}^{(n)}$ recursively, considering one additional TFBS at each step. Note that if two different TFs bind to exactly the same location on a cis-regulatory region, we treat this as two TFBSs, not as one, and treat first one and then the other in our recursive algorithm.

Consider the case where the (n+1)$^{\mathrm{th}}$ binding site belongs to an activator. The case where this activator is not bound contributes $P_{A,R}^{(n)} P_\mathrm{u}(n+1)$ to $P_{A,R}^{(n+1)}$. If it is bound, then we must also take into account that the (n+1)$^{\mathrm{th}}$ binding site overlaps (partially or completely) with the last $H \geq 0$ sites, and so contributes $P_{A-1,R}^{(n-H)} P_\mathrm{b}(n+1) \prod_{j=n-H+1}^{n} P_\mathrm{u}(j)$. Taken together,

$$P_{A,R}^{(n+1)} = P_{A,R}^{(n)} P_\mathrm{u}(n+1) + P_{A-1,R}^{(n-H)} P_\mathrm{b}(n+1) \prod_{j=n-H+1}^{n} P_\mathrm{u}(j). \quad (5)$$

Similarly, if the (n+1)$^{\mathrm{th}}$ site belongs to a repressor, we have

$$P_{A,R}^{(n+1)} = P_{A,R}^{(n)} P_\mathrm{u}(n+1) + P_{A,R-1}^{(n-H)} P_\mathrm{b}(n+1) \prod_{j=n-H+1}^{n} P_\mathrm{u}(j). \quad (6)$$

By definition, $P_{A,R}^{(n)} = 0$ for binding configurations that are impossible, e.g. those with negative *A* or negative *R*. We initialize the recursion at $n = 0$, where the only valid binding configuration is for $A = R = 0$, i.e. $P_{0,0}^{(0)} = 1$. At $n = 1$, $P_{0,0}^{(1)} \propto P_\mathrm{u}(1)$ and if the binding site belongs to an activator $P_{1,0}^{(1)} \propto P_\mathrm{b}(1)$;

otherwise, $P_{1,0}^{(1)} \propto P_{\mathrm{b}}(1)$. For a gene where the total number N of TFBSs is 1, $P_{0,0}^{(1)}$, $P_{1,0}^{(1)}$, and $P_{0,1}^{(1)}$ sum to 1 and normalization is unnecessary. For higher values of $N = N_{\mathrm{Act}} + N_{\mathrm{Rep}}$ TFBSs, where N_{Act} and N_{Rep} are the total numbers of activator binding sites and repressor binding sites, respectively, we normalize $P_{A,R}^{(N)}$ at the end of the recursion by dividing by $\sum_{A=0}^{N_{\mathrm{Act}}} \sum_{R=0}^{N_{\mathrm{Rep}}} P_{A,R}^{(N)}$ to get the probability of binding configurations that include exactly A activators and R repressors.

$r_{\mathrm{Act\_to\_Int}}$

Transcription initiation over an interval of time $r_{\mathrm{transc\_init}}$ is proportional to the proportion of time spent in the Active state. Assuming a steady state between Repressed, Intermediate, and Active states, as a function of current TF concentrations, we have:

$$\frac{r_{\mathrm{transc\_init}}}{r_{\mathrm{max\_transc\_init}}} = \frac{r_{\mathrm{Int\_to\_Act}}}{r_{\mathrm{Int\_to\_Act}} + r_{\mathrm{Act\_to\_Int}}} P_{\mathrm{Int\_or\_Act}}, \quad (7)$$

where $P_{\mathrm{Int\_or\_Act}}$ is the probability a gene is at Intermediate or Active. We set $r_{\mathrm{max\_transc\_init}}$ (the rate of transcription given 100% Active state) to 6.75 min^{-1}, based on the corresponding rate when a model of the *PHO5* promoter is fit to data (Brown et al. 2013). In this model fit, the constitutively expressed *PHO5* promoter is free of nucleosomes 80% of the time, i.e. $P_{\mathrm{Int\_or\_Act}} = 0.8$. We take these two values as universal for constitutively expressed genes, and assume that variation in $r_{\mathrm{Act\_to\_Int}}$ is responsible for variation in $r_{\mathrm{transc\_init}}$. To identify a set of constitutively expressed genes, we identified 225 genes that have mRNA production rate of at least 0.5 molecule min^{-1} from genome-wide measurements (Pelechano et al. 2010); this threshold corresponds to low H2A.Z occupancy (Guillemette et al. 2005). We set $r_{\mathrm{transc\_init}}$ to the production rate of mRNA of these 225 genes, and solve for gene-specific $r_{\mathrm{Act\_to\_Int}}$ from Eq. S7. We fit the solutions to a log-normal distribution and arrive at $10^{\mathrm{N}(1.27,\ 0.226)}$ min^{-1}.

To initialize values of $r_{\mathrm{Act\_to\_Int}}$ for each gene, we sample from this distribution. We also set lower and upper bounds for allowable values; if either the initial sample or subsequent mutation put $r_{\mathrm{Act\_to\_Int}}$ beyond these bounds, we set the value of $r_{\mathrm{Act\_to\_Int}}$ to equal to boundary value. We set the lower bound for $r_{\mathrm{Act\_to\_Int}}$ at 0.59 min^{-1}, half the minimum of the values inferred from the set of 225 genes. To set an upper bound, we use the low H2A.Z occupancy bound of $r_{\mathrm{transc\_init}} = 0.5$, which gives a solution of 32.34 min^{-1}; we double this to set the upper bound as 64.7 min^{-1}.

Transcription delay times

Yeast protein lengths fit a log-normal distribution of $10^{\mathrm{N}(2.568,\ 0.34)}$ amino acids (from the Saccharomyces Genome Database (SGD Project), excluding mitochondrial proteins; YeastMine (Balakrishnan et al. 2012) was used to query the database and to download data). We sample ORF length L from this distribution. To constrain the values of L, we set a lower bound of 50 amino acids and an upper bound of 5,000 amino acids; the longest protein in SGD is 4910 amino acids. If either initialization or mutation put L beyond these bounds, we set the value of L to the boundary value.

With an mRNA elongation rate of 600 codon per min (Larson et al. 2011; Hocine et al. 2013), it takes L / 600 minutes to transcribe the ORF of an mRNA. Also including time for transcribing UTRs and for transcription termination, and ignoring introns for simplicity, it takes 290 seconds to complete transcription of the yeast *GLT1* gene (Larson et al. 2011), whose ORF is 6.4kb. Putting the two together, we infer that transcribing the UTRs and terminating transcription takes around 1 minute for *GLT1*.

Generalizing to assume that transcribing UTRs and terminating transcription takes exactly 1 minute for all genes, producing an mRNA from a gene of length L takes $1 + L / 600$ minutes.

Translation delay times and $r_{protein\_syn}$

We model a second delay between the completion of a transcript and the production of the first protein from it. The delay comes from a combination of translation initiation and elongation; it ends when the mRNA is fully loaded with ribosomes all the way through to the stop codon and the first protein is produced. We ignore the time required for mRNA splicing; introns are rare in yeast (Dujon 1996). mRNA transportation from nucleus to cytosol, which is likely diffusion-limited (Niño et al. 2013; Smith et al. 2015), is fast even in mammalian cells (Mor et al. 2010) let alone much smaller yeast cells, and the time it takes is also ignored. The median time in yeast for initiating translation is 0.5 minute (Table 1 in Siwiak et al. 2010), and the genomic average peptide elongation rate is 330 codon/min (Siwiak et al. 2010). After an mRNA is produced, we therefore wait for $0.5 + L / 330$ minutes, and then model protein production as continuous at a gene-specific rate $r_{protein\_syn}$.

To calculate $r_{protein\_syn}$, we combine the gene-specific ribosome densities D along the mRNAs and the gene-specific peptide elongation rates E, both measured in yeast (Siwiak et al. 2010). The values of DE across yeast genes fit the log-normal distribution $10^{N(0.322,\ 0.416)}$ molecule mRNA^{-1} min^{-1}; we initialize $r_{protein\_syn}$ for each gene by sampling from this distribution. We set the lower bound for $r_{protein\_syn}$ at half the minimum observed value of DE (4.5×10^{-3} molecule mRNA^{-1} min^{-1}). The upper bound corresponds to an mRNA fully occupied by rapidly moving ribosomes. Each ribosome occupies about 10 codons (Siwiak et al. 2010), and the peptide elongation rate can be as high as 614 codon per min (Waldron et al. 1977). If ribosomes are packed closely together at 10 codons apart, a protein comes off the end of production in the time taken to elongate 10 codons, i.e. proteins are produced at 61.4 molecules per minute. If either initialization or mutation put $r_{protein\_syn}$ beyond these bounds, we set the value of $r_{protein\_syn}$ to the boundary value.

mRNA and protein decay rates

We fit a log-normal distribution $10^{N(-1.49,\ 0.267)}$ min^{-1} to yeast mRNA degradation rates (Wang et al. 2002), and initialize the mRNA degradation rate r_{mRNA_deg} for each gene by sampling from this distribution. We set lower and upper bounds for r_{mRNA_deg} at half the minimum and twice the maximum observed values (7.5×10^{-4} min^{-1} and 0.54 min^{-1}), respectively. If either initialization or mutation put r_{mRNA_deg} beyond these bounds, we set the value of r_{mRNA_deg} to the boundary value.

Expressing the estimated half-lives of yeast proteins (Belle et al. 2006) in terms of protein degradation rates, they fit the log-normal distribution $10^{N(-1.88,\ 0.56)}$ min^{-1}; we initialize gene-specific protein degradation rates $r_{protein\_deg}$ by sampling from this distribution. We ignore the additional reduction in protein concentration due to dilution as the cell grows and thus increases in volume. We set lower and upper bounds for $r_{protein\_deg}$ at half the minimum and twice the maximum observed degradation rate (3×10^{-6} min^{-1} and 0.69 min^{-1}), respectively. If either initialization or mutation put $r_{protein\_deg}$ beyond these bounds, we set the value of $r_{protein\_deg}$ to the boundary value.

Simulation of gene expression

Our algorithm is part-stochastic, part-deterministic. We use a Gillespie algorithm (Gillespie 1977) to simulate stochastic transitions between Repressed, Intermediate, and Active chromatin states, and to

simulate transcription initiation and mRNA decay events. We refer to these as "Gillespie events". The completion of transcription to produce a complete mRNA, and subsequent ribosomal loading onto the mRNA, are referred to as "fixed events" (they require fixed times of 1 + *L* / 600 minutes and 0.5 + *L* / 330 minutes, respectively). Scheduled changes in the strength of the external signal are also fixed events. Protein production and degradation are described deterministically with ODEs, and updated frequently in order to recalculate TF concentrations and hence chromatic transition rates. Updates occur at the time of Gillespie and fixed events, and also in between as described later below.

The total rate of all Gillespie events is

$$r_{\text{total}} = \sum_{i=1}^{\text{Rep}} r_{\text{Rep\_to\_Int\_i}} + \sum_{i=1}^{\text{Int}} (r_{\text{Int\_to\_Rep\_i}} + r_{\text{Int\_to\_Act\_i}}) + \sum_{i=1}^{\text{Act}} (r_{\text{Act\_to\_Int\_i}} + r_{\text{transc}}) + \sum_{i=1}^{N_{\text{copies}}} r_{\text{mRNA\_deg\_i}} N_{\text{mRNA\_i}}, \quad (8)$$

where Rep, Int, and Act are the numbers of gene copies in our haploid model that are in the Repressed, Intermediate, and Active chromatin states, respectively, $N_{\text{mRNA\_i}}$ is the number of completely transcribed mRNA molecules from gene *i*, and N_{copies} is the total number of gene copies. We only simulate degradation of full transcribed mRNA, and not that of mRNA that are still being transcribed, because the latter are already captured implicitly by $r_{\text{max\_transc\_init}}$, which is based on mRNAs that complete transcription (Brown et al. 2013). Once an mRNA finishes transcription, it is subjected to degradation regardless of whether ribosome loading is complete.

The waiting time Δt_G before the next Gillespie event is

$$\Delta t_G = \frac{x}{r_{\text{total}}}, \quad (9)$$

where *x* is random number drawn from an exponential distribution with mean 1. Which Gillespie event takes place next is sampled only if a different update does not happen first. If a fixed event is scheduled to happen first at $\Delta t_F < \Delta t_G$, we advance time by Δt_F, update the state of the cell, and calculate a new r_{total}'. Since the cellular activity has been going on with the old rate r_{total} for Δt_F, the remaining "labor" required to trigger the Gillespie event planned earlier is reduced. The new waiting time, $\Delta t_G'$, to trigger the planned Gillespie event is

$$\Delta t_G' = \frac{x - r_{\text{total}} \Delta t_F}{r_{\text{total}}'}. \quad (10)$$

Gene duplication creates $n \geq 1$ genes copies producing the same protein, where each copy *i* might have diverged in their production rate $r_{\text{protein\_syn\_i}}$ and degradation rate $r_{\text{protein\_deg\_i}}$. Complete proteins are produced continuously once an mRNA molecule is fully loaded with ribosomes, which occurs 0.5 + *L* / 330 minutes after transcription is complete – the concentration of such molecules is denoted $N_{\text{mRNA\_aft\_delay\_i}}(t)$. The total concentration of a protein obeys:

$$N'_{\text{protein}}(t) = \sum_i^n \left(r_{\text{protein\_syn\_i}} N_{\text{mRNA\_aft\_delay\_i}}(t) - r_{\text{protein\_deg\_i}} N_{\text{protein\_i}}(t) \right) \quad (11)$$

Protein concentrations are updated using a closed-form integral of Supplementary Equation 11

$$N_{\text{protein}}(t_1) = \sum_i^n \left(\frac{r_{\text{protein\_syn\_i}} N_{\text{mRNA\_aft\_delay\_i}}}{r_{\text{protein\_deg\_i}}} + \left(N_{\text{protein\_i}}(t_0) - \frac{r_{\text{protein\_syn\_i}} N_{\text{mRNA\_aft\_delay\_i}}}{r_{\text{protein\_deg\_i}}}\right) e^{-r_{\text{protein\_deg\_i}}(t_1 - t_0)}\right) \quad (12)$$

with this expression updated every time a Gillespie or fixed event at time t_1 changes the value of $N_{\text{mRNA\_aft\_delay\_i}}$.

In between updates, values of P_A, P_R, $P_{A\_no\_R}$, and $P_{notA\_no\_R}$, and hence chromatin transition rates, are calculated under the approximation of constant N_{protein}. Additional updates, above and beyond fixed and Gillespie events, are performed in order to ensure that chromatin transition rates do not change too dramatically from one update to the next. We use a target of D = 0.01 for the amount of change tolerated in the values of P_A, P_R, $P_{A\_no\_R}$, and $P_{notA\_no\_R}$, in order to schedule updates after time Δt_U, which are triggered when neither a Gillespie event nor a fixed event occurs before this time has elapsed, i.e. when $\Delta t_U < \Delta t_F$ and $\Delta t_U < \Delta t_G$.

There is the greatest potential for large changes after an update that changes the value of $N_{\text{mRNA\_aft\_delay\_i}}$. In this case, we solve for the time interval for which the probability that TF i would be bound to a single perfect and non-overlapping TFBS would change by D, by choosing $\Delta t_U > 0$ that satisfies

$$\left| \frac{N_i(t)}{N_i(t) + \bar{K}_{\text{d\_i}}(0)} - \frac{N_i(t + \Delta t_U)}{N_i(t + \Delta t_U) + \bar{K}_{\text{d\_i}}(0)} \right| = D. \quad (13)$$

where the two left-hand terms are derived from Supplementary Equation 4. A solution for Δt_U may not exist, e.g. if the concentration of TF i is decreasing but $P_{\text{b\_i}}(t) < D$. In such cases, we set Δt_U to infinity.

When the previous update does not change any $N_{\text{mRNA\_aft\_delay\_i}}$ values, then we modify Δt_U adaptively. Let d be the maximum of ΔP_A, ΔP_R, $\Delta P_{A\_no\_R}$, and $\Delta P_{notA\_no\_R}$ during the last update, and Δt be the advance in time between the last two updates. We then schedule an update at

$$\Delta t_U' = \frac{D}{d} \Delta t. \quad (14)$$

After an update that changes the value of $N_{\text{mRNA\_aft\_delay\_i}}$, we use the smaller value from Supplementary Equations 13 and 14. These additional update times are discarded and recalculated when a Gillespie or fixed event occurs first. Supplementary Figure 12 of Xiong et al. (2019) shows that simulations rarely exceed the target of D = 0.01, and do so only modestly.

Cost of gene expression

The cost of gene expression comes from some combination of the act of expression and from the presence of the resulting gene product. Yeast cells with plasmids carrying fast-degrading GFP had as much growth impairment as those carrying wild-type GFP (Fig. 3 of Kafri et al. 2016), suggesting that the former cost dominates. Universal costs stemming from the act of gene expression include the consumption of energy (Wagner 2005; Wagner 2007) and the opportunity cost of not using ribosomes to make other gene products (Scott et al. 2014). While some costs arise from transcription (Kafri et al. 2016), we simplify our model by attributing all of the cost of expression to the act of translation.

Kafri et al. (2016) reported that, in rich media, the growth rate of haploid yeast is reduced by about 1% when mCherry is expressed to about 2% of proteome. Setting the growth rate of the yeast when mCherry is not expressed, i.e. the fitness, to one, we have the cost of gene expression equal to 0.01. Next, we estimate the production rate of mCherry in Kafri et al. (2016) by assuming that mCherry is in steady state between production and dilution due to cell division; fluorescent proteins tend to be stable such that degradation can be ignored (Snapp 2009). Ghaemmaghami et al. (2003) estimated that a haploid yeast cell contains about 5×10^7 protein molecules, 2% of which are now mCherry. Over a 90 minute cell cycle in Kafri et al. (2016), about 5×10^5 mCherry molecule per cell need to be expressed in order to double in numbers. This yields a production rate of about 5×10^3 mCherry molecules per minute per cell. Because the total cost of gene expression is 0.01, the cost at a protein production rate of one mCherry molecule per minute per cell, c_{transl}, is 2×10^6. Long genes should be more expensive to express than short ones; for a gene of length L, we assume its cost of expression is $c_{\text{transl}}L$ / 370, where 370 is the geometric mean length of a yeast protein as described above in "Transcription delay times". Results using the length of mCherry instead, i.e. a slightly higher cost of expression of $c_{\text{transl}}L$ / 236, are unlikely to be significantly different.

The overall cost of gene expression at time t, $C(t)$ is:

$$C(t) = c_{\text{transl}}\left(\sum_{i=1}^{N_{\text{copies}}} \frac{L_i}{10^{2.568}} r_{\text{transl\_init\_i}} N_{\text{mRNA\_aft\_delay\_i}}(t) + \sum_{i=1}^{N_{\text{copies}}} \frac{L_i}{10^{2.568}} \frac{r_{\text{transl\_init\_i}}}{2} N_{\text{mRNA\_during\_delay\_i}}(t)\right). \quad (15)$$

The second term represents transcripts that are on average half-loaded with ribosomes, and hence experiencing on average half the cost of translation. We integrate $C(t)$ within segments of constant $C(t)$ to obtain the overall cost of gene expression during a simulation.

Mutation

Because we use an origin-fixation approach, only the relative and not the absolute values of our mutation rates matter. In *S. cerevisiae,* the rates of small indels and of single nucleotide substitutions have been estimated as 0.2×10^{-10} per base pair and 3.3×10^{-10} per base pair, respectively (Lynch et al. 2008). Thus, cis-regulatory sequences are primarily shaped by single nucleotide substitutions. We do not model small indels in the cis-regulatory sequence, but increase the single nucleotide substitution up to 3.5×10^{-10} per base pair to compensate. This corresponds to a rate of 5.25×10^{-8} per 150 bp cis-regulatory sequence.

Lynch et al. (2008) also report a rate of gene duplication of 1.5×10^{-6} per gene and of deletion of 1.3×10^{-6} per gene (not including non-deletion-based loss of function mutations). These values turned out to swamp the evolution of TFBSs and hence significantly slow down our simulations, so we chose values 10-fold lower, making both gene duplication and gene deletion occur at rate 1.5×10^{-7} per gene. This preserves their numerical excess but reduces its magnitude.

Our model contains 8 gene-specific parameters, namely L, $r_{\text{Act\_to\_Int}}$, $r_{\text{protein\_deg}}$, $r_{\text{protein\_syn}}$, $r_{\text{mRNA\_deg}}$, the $K_d(0)$ of a TF, whether a TF is an activator vs. repressor, and the consensus binding sequence of a TF. We assume mutations to L are caused by relatively neutral small indels, which we assume to be 20% of all small indels; mutation to L therefore occurs at rate 1.2×10^{-11} per codon, i.e. $1.2 \times 10^{-11}L$ for a gene of length L. For $r_{\text{Act\_to\_Int}}$, we assume that it is altered by 10% of all the point mutations (single nucleotide substitution and small indels) to the core promoter of a gene. The length of a core promoter is about

100 bp and is relatively constant among genes (Roy and Singer 2015), yielding a mutation rate of $r_{\text{Act\_to\_Int}}$ of 3.5×10^{-9} per gene.

The remaining 6 gene-specific parameter mutation rates are parameterized with lower accuracy due to lack to data; the principal decision is which to make dependent vs. independent of gene length. TF binding to DNA depends on particular peptide motifs whose length is likely independent of TF length, therefore we make mutation rates independent of gene length for mutations to $K_d(0)$, to the consensus binding sequence of a TF, and to the activating vs repressing identity of a TF. We set the rate of each of the three mutation types to 3.5×10^{-9} per gene. In contrast, because the stability of an mRNA mainly depends on its codon usage (Cheng et al. 2017) and thus more codons means more opportunities for change, we assume the rate of mutation to $r_{\text{mRNA\_deg}}$ does depend on gene length, as do mutations to protein stability $r_{\text{protein\_deg}}$. $r_{\text{protein\_syn}}$ is determined by the density of ribosomes on mRNA and the elongation rate of ribosomes, and therefore is affected both by ribosome loading speed and by slow spots forming queues in the mRNA. Ribosome loading often relies on the 5'UTR of mRNA (Hinnebusch 2011), and 5'UTR length is positively correlated with ORF length (Tuller et al. 2009). Slow-spots in mRNA can be due to secondary structure or to suboptimal codons, therefore are also more likely to appear by mutation to long mRNAs, so we assume the rate of mutation to $r_{\text{protein\_syn}}$ depends on gene length. We set the mutation rates of $r_{\text{protein\_deg}}$, $r_{\text{protein\_syn}}$, and $r_{\text{mRNA\_deg}}$ each to 9.5×10^{-12} per codon; in other words, each mutation rate is 3.5×10^{-9} for a yeast gene of average length (on a log-scale) $10^{2.568}$ = 370 codons.

$r_{\text{Act\_to\_Int}}$, $r_{\text{protein\_syn}}$, $K_d(0)$, $r_{\text{protein\_deg}}$, and $r_{\text{mRNA\_deg}}$ evolve as quantitative traits. They are assumed to have, in the absence of selection, a log-normal stationary distribution with mean μ and standard deviation σ, with values estimated below and listed in Supplementary Table 2. Denote the values of a parameter as x before mutation and x' after mutation; mutation takes the form:

$$\log_{10} x' = \log_{10} x + \text{Normal}(k(\mu - \log_{10} x), \sigma), \tag{16}$$

where k controls the speed of regressing back to the stationary distribution; we set k = 0.5 for all 5 parameters. To set values of μ, central tendency estimates of these five values (from Supplementary Table 1**)** are adjusted according to our expectations about mutation bias. We assume a mutation bias toward faster mRNA degradation $r_{\text{mRNA\_deg}}$, faster $r_{\text{Act\_to\_Int}}$ (Decker and Hinton 2013; Roy and Singer 2015), slower translation initiation $r_{\text{protein\_syn}}$ (Hinnebusch 2011), and larger $K_d(0)$. We assume that the observed log-normal means of $r_{\text{mRNA\_deg}}$, $r_{\text{protein\_syn}}$, and $r_{\text{Act\_to\_Int}}$ differ by 2-fold from the mean expected from mutational bias; for example, the mean of $\log_{10}(r_{\text{mRNA\_deg}})$ is -1.49, so the value of μ for $r_{\text{mRNA\_deg}}$ is -1.49 + $\log_{10}(2)$ = -1.19. We assume a larger bias for $K_d(0)$, namely that mutation is likely to reduce the affinity of a TF for a TFBS down to non-specific levels. Thus, we set $\mu = \log_{10}(K_d(3)) = -5$ for $K_d(0)$; note that in this case μ is equal to one of the boundary values, which will be hit far more often than during the evolution of other parameters. We assume that the observed central tendency estimate of protein stability does not depart from mutational equilibrium, therefore the value of μ for $r_{\text{protein\_deg}}$ is the mean of $\log_{10}(r_{\text{protein\_deg}})$ = -1.88.

The value of σ controls mutational effect size. We set the value of σ such that 1% of mutational changes from $x = 10^{\mu}$ go beyond the boundary values, for simplicity approximating by considering only the closer of the two boundary values on a log scale, i.e. we solve Supplementary Equation 17 for σ:

$$\begin{cases} P(\mu + \text{Normal}(0, \sigma) \geq \log_{10} B_{\text{U}}) = 0.01, \text{if the upper bound } B_{\text{U}} \text{ is closer} \\ P(\mu + \text{Normal}(0, \sigma) \leq \log_{10} B_{\text{L}}) = 0.01, \text{if the lower bound } B_{\text{L}} \text{ is closer} \end{cases} \tag{17}$$

For example, the upper and the lower bounds of r_{mRNA_deg} are 0.54 min^{-1} and 7.5×10^{-4} min^{-1}; on a log-scale, the upper bound is closer to $10^{\mu} = 10^{-1.19}$ min^{-1}. Plugging these values in Eq. S8 and solving for σ, we have $\sigma = 0.396$. We set the values of σ for $r_{protein\_syn}$, and $r_{protein\_deg}$ in the same way. However for $r_{Act\_to\_Int}$, σ is set according to the lower bound, even though it is the more distant from 10^{μ}, because otherwise a stable preinitiation complex will evolve too rarely. Under this high mutational variance, evolutionary outcomes at the two bounds are still only observed 5% of the time. For $K_d(0)$, because its upper bound is equal to 10^{μ}, we set σ to 0.776, such that 1% of mutations can change the values of $K_d(0)$ by 100-fold or more.

Mutant values of L, $r_{Act\_to\_Int}$, $r_{protein\_syn}$, $r_{protein\_deg}$, and r_{mRNA_deg} are constrained by the same bounds that constrain the initial values of these parameters (see previous sections). If a mutation increases the value of any of these 5 parameters to beyond the corresponding upper bound, we set the mutant value to the upper bound; similarly for a mutant value that is smaller than the lower bound of the corresponding parameter. For mutation to $K_d(0)$, we resample if $x' \geq K_d(3)$, because otherwise the mutation effectively "deletes" the TF by reducing its affinity to non-specific levels.

References

Balakrishnan R, Park J, Karra K, Hitz BC, Binkley G et al. . 2012. YeastMine—an integrated data warehouse for *Saccharomyces cerevisiae* data as a multipurpose tool-kit. Database:bar062.

Belle A, Tanay A, Bitincka L, Shamir R, O'Shea EK. 2006. Quantification of protein half-lives in the budding yeast proteome. PNAS 103(35):13004-13009.

Benos PV, Bulyk ML, Stormo GD. 2002. Additivity in protein-DNA interactions: how good an approximation is it? Nucleic Acids Research 30(20):4442-4451.

Brown CR, Mao C, Falkovskaia E, Jurica MS, Boeger H. 2013. Linking Stochastic Fluctuations in Chromatin Structure and Gene Expression. PLoS Biology 11(8):e1001621.

Cheng J, Maier KC, Avsec Ž, Rus P, Gagneur J. 2017. Cis-regulatory elements explain most of the mRNA stability variation across genes in yeast. RNA 23(11):1648-1659.

Decker KB, Hinton DM. 2013. Transcription Regulation at the Core: Similarities Among Bacterial, Archaeal, and Eukaryotic RNA Polymerases. Annu. Rev. Microbiol 67:113-139.

Dujon B. 1996. The yeast genome project: what did we learn? Trends in Genetics 12(7):263-270.

Ghaemmaghami S, Huh W-K, Bower K, Howson RW, Belle A et al. . 2003. Global analysis of protein expression in yeast. Nature 425(6959):737-741.

Gillespie DT. 1977. Exact stochastic simulation of coupled chemical reactions. Journal of Physical Chemistry 81(25):2340-2361.

Guillemette B, Bataille AR, Gevry N, Adam M, Blanchette M et al. . 2005. Variant histone H2A.Z is globally localized to the promoters of inactive yeast genes and regulates nucleosome positioning. PLoS Biol 3(12):e384.

Hinnebusch AG. 2011. Molecular Mechanism of Scanning and Start Codon Selection in Eukaryotes. Microbiology and Molecular Biology Reviews 75(3):434-467.

Hocine S, Raymond P, Zenklusen D, Chao JA, Singer RH. 2013. Single-molecule analysis of gene expression using two-color RNA labeling in live yeast. Nature Methods 10(2):119-121.

Kafri M, Metzl-Raz E, Jona G, Barkai N. 2016. The Cost of Protein Production. Cell Reports 14(1):22-31.

Katan-Khaykovich Y, Struhl K. 2002. Dynamics of global histone acetylation and deacetylation in vivo: rapid restoration of normal histone acetylation status upon removal of activators and repressors. Genes & development 16(6):743-52.

1430 Larson DR, Zenklusen D, Wu B, Chao JA, Singer RH. 2011. Real-time observation of transcription
1431 initiation and elongation on an endogenous yeast gene. Science 332(6028):475-478.
1432 Lee W, Tillo D, Bray N, Morse RH, Davis RW et al. . 2007. A high-resolution atlas of nucleosome
1433 occupancy in yeast. Nature Genetics 39(10):1235-44.
1434 Lynch M, Sung W, Morris K, Coffey N, Landry CR et al. . 2008. A genome-wide view of the spectrum of
1435 spontaneous mutations in yeast. Proceedings of the National Academy of Sciences of the United
1436 States of America 105:9272-9277.
1437 Maerkl SJ, Quake SR. 2007. A Systems Approach to Measuring the Binding Energy Landscapes of
1438 Transcription Factors. Science 315(5809):233-237.
1439 Mor A, Suliman S, Ben-Yishay R, Yunger S, Brody Y et al. . 2010. Dynamics of single mRNP
1440 nucleocytoplasmic transport and export through the nuclear pore in living cells. Nature Cell
1441 Biology 12(6):543-552.
1442 Nalefski EA, Nebelitsky E, Lloyd JA, Gullans SR. 2006. Single-molecule detection of transcription factor
1443 binding to DNA in real time: Specificity, equilibrium, and kinetic parameters. Biochemistry
1444 45(46):13794-13806.
1445 Niño CA, Hérissant L, Babour A, Dargemont C. 2013. mRNA nuclear export in yeast. Chemical Reviews
1446 113(11):8523-8545.
1447 Park S, Chung S, Kim KM, Jung KC, Park C et al. . 2004. Determination of binding constant of transcription
1448 factor myc-max/max-max and E-box DNA: The effect of inhibitors on the binding. Biochimica et
1449 Biophysica Acta - General Subjects 1670(3):217-228.
1450 Pelechano V, Chávez S, Pérez-Ortín JE. 2010. A Complete Set of Nascent Transcription Rates for Yeast
1451 Genes. PLoS ONE 5(11):e115560.
1452 Roy AL, Singer DS. 2015. Core promoters in transcription: old problem, new insights. Trends in
1453 Biochemical Sciences 40(3):165-171.
1454 Scott M, Klumpp S, Mateescu EM, Hwa T. 2014. Emergence of robust growth laws from optimal
1455 regulation of ribosome synthesis. Molecular Systems Biology 10(8):747.
1456 SGD Project. Available from: https://yeastmine.yeastgenome.org
1457 Siwiak M, Zielenkiewicz P, Jacobson A, Grebogi C, Kito K. 2010. A Comprehensive, Quantitative, and
1458 Genome-Wide Model of Translation. PLoS Computational Biology 6(7):e1000865.
1459 Smith C, Lari A, Derrer CP, Ouwehand A, Rossouw A et al. . 2015. In vivo single-particle imaging of
1460 nuclear mRNA export in budding yeast demonstrates an essential role for Mex67p. Journal of
1461 Cell Biology 211(6):1121-1130.
1462 Snapp EL. 2009. Fluorescent proteins: a cell biologist's user guide. Trends in Cell Biology 19(11):649-655.
1463 Tuller T, Ruppin E, Kupiec M. 2009. Properties of untranslated regions of the *S. cerevisiae* genome. BMC
1464 Genomics 10:391.
1465 Wagner A. 2005. Energy constraints on the evolution of gene expression. Molecular Biology and
1466 Evolution 22(6):1365-1374.
1467 Wagner A. 2007. Energy costs constrain the evolution of gene expression. Journal of Experimental
1468 Zoology Part B-Molecular and Developmental Evolution 308B(3):322-324.
1469 Waldron C, Jund R, Lacroute F. 1977. Evidence for a high proportion of inactive ribosomes in slow-
1470 growing yeast cells. Biochemical Journal 168(3):409-415.
1471 Wang M, Herrmann CJ, Simonovic M, Szklarczyk D, von Mering C. 2015. Version 4.0 of PaxDb: Protein
1472 abundance data, integrated across model organisms, tissues, and cell-lines. Proteomics
1473 15(18):3163-3168.
1474 Wang Y, Liu CL, Storey JD, Tibshirani RJ, Herschlag D et al. . 2002. Precision and functional specificity in
1475 mRNA decay. Proceedings of the National Academy of Sciences of the United States of America
1476 99(9):5860-5865.

1477 Wunderlich Z, Mirny LA. 2009. Different gene regulation strategies revealed by analysis of binding
1478 motifs. Trends in Genetics 25(10):434-440.
1479 Xiong K, Lancaster AK, Siegal ML, Masel J. 2019. Feed-forward regulation adaptively evolves via
1480 dynamics rather than topology when there is intrinsic noise. Nature Communications
1481 10(1):2418.
1482 Yuan GC, Liu YJ, Dion MF, Slack MD, Wu LF et al. . 2005. Genome-scale identification of nucleosome
1483 positions in S. cerevisiae. Science 309(5734):626-30.
1484 Zhu J, Zhang MQ. 1999. SCPD: a promoter database of the yeast *Saccharomyces cerevisiae*.
1485 Bioinformatics 15(7):607-611.

1486